Plasma-catalytic partial oxidation of methane on Pt(111) : a microkinetic study on the role of different plasma species

Plasma-catalytic partial oxidation of methane on Pt(111): a microkinetic study of the role of different plasma species

Björn Loenders*, Yannick Engelmann and Annemie Bogaerts
Research group PLASMANT, Department of Chemistry, University of Antwerp,
Universiteitsplein 1, B-2610 Wilrijk-Antwerp, Belgium
*E-mail: bjorn.loenders@uantwerpen.be

Abstract

We use microkinetic modelling to examine the potential of plasma-catalytic partial oxidation (POX) of CH_4 as a promising new approach to produce oxygenates. We study how different plasma species affect POX of CH_4 on a Pt(111) surface and we discuss the associated kinetic and mechanistic changes. We discuss the effect of vibrationally excited CH_4 and O_2, as well as plasma-generated radicals and stable intermediates. Our results show that vibrational excitation enhances the turnover frequency (TOF) of catalytic CH_4 dissociation and has good potential for improving the selectivities towards CH_3OH, HCOOH and C_2 hydrocarbons. Nevertheless, when also considering plasma-generated radicals, we find that these species mainly govern the surface chemistry. Additionally, we find that plasma-generated radicals and stable intermediates enhance the TOFs of CO_x and oxygenates, increase the selectivity towards oxygenates and make the formation of HCOOH more significant on Pt(111). We also briefly illustrate the potential impact of Eley-Rideal reactions that involve plasma-generated radicals. Finally, we reveal how various radicals affect the catalyst surface chemistry and we link this to the formation of the different products. This allows us to make suggestions of how the plasma composition should be altered in order to improve the formation of the desired products.

Keywords

Partial oxidation of CH_4, Plasma catalysis, Microkinetic modelling, Vibrational excitation, Radicals

1. Introduction

The remote locations of many natural gas reserves and the difficulties associated with transporting methane (CH_4) ask for technologies that convert CH_4 into liquid chemicals prior to transportation, to make its valorisation economically attractive. Such technologies would transform an important greenhouse gas, while simultaneously decreasing the dependency on oil for production of chemicals and fuels.[1–3] The partial oxidation (POX) of CH_4 into liquid oxygenates is therefore a particularly interesting route for CH_4 conversion.[4,5] Yet, certain challenges are associated with this approach, such as breaking the strong C-H bond in CH_4, while avoiding deep oxidation of the oxygenates to CO and CO_2.[6,7] In classical thermal catalysis, the POX of CH_4 has therefore been mainly investigated for syngas production at high temperatures with transition metal catalysts, like Ru, Rh, Ni and Pt.[8]

Non-thermal plasma (NTP) offers a distinct approach for easier breaking of the C-H bond in CH_4 compared to thermal catalysis. NTP is characterised by highly energetic electrons, which can provide the energy required to induce chemical reactions, and thus the use of high gas temperatures can be avoided. On the other hand, the high reactivity of plasma can hamper the selective formation of the desired products.[9,10] The selectivity of NTP can be improved by combining it with a catalyst, as is done in plasma catalysis. The various reactive species formed in NTP (radials, excited molecules, etc.) can adsorb onto the catalyst, which directs their further reaction towards the desired products. Needless to say, good knowledge of the interaction between the plasma species and the catalyst is required to select the optimal catalyst material and operating conditions.[11–13]

The POX of CH_4 has been investigated in a variety of plasma reactors.[4,9,14–20] Among these the dielectric barrier discharge (DBD) reactor is most common, as it can be easily operated at atmospheric pressure and scaled up for industrial use.[21] Some selectivity towards organic oxygenates (CH_3OH, CH_2O, HCOOH, etc.) can be achieved by POX of CH_4 in a DBD, but large amounts of CO and CO_2 are also formed. As a result, further increase in oxygenate selectivity is an important issue.[4] Combination of a DBD plasma with the correct catalyst might solve this issue.

Various experimental works have investigated how the conversions and selectivities in POX of CH_4 are altered when combining a plasma with a wide variety of catalyst materials, including but not limited to: CuO-based catalyst,[22–24] Fe_2O_3,[25,26] Mn oxides,[26] copper-zinc-alumina doped with various metals,[27,28], NiO,[26,29] Ni,[29–31], Pt,[25,30] Pd,[32] Fe[32] and Mo.[32] While these studies offer

useful information, they usually provide limited insight, due to the complexity of the plasma-catalytic system, resulting from the various interactions at play. As a result, a detailed fundamental understanding of the plasma-catalytic surface chemistry, for POX of CH_4 as well as other reactions, is still lacking.[11–13]

Only a few mechanistic studies are available on the surface chemistry for the plasma-catalytic oxidation of CH_4. Knoll *et al.*[33] investigated POX of CH_4 by an Ar/O_2 atmospheric pressure plasma jet (APPJ) in the presence of a Ni on Al_2O_3/SiO_2 catalyst, using *in situ* diffuse reflectance infrared Fourier transform spectroscopy (DRIFTS). The authors find that CO_2 formation is enhanced at higher temperature and that CO is likely being converted to CO_2 on the catalyst surface. However, they also suggest the presence of carboxylate groups or COO^-, which are likely precursors to CO_2.[33] Zhang *et al.*[34] investigated the decomposition and oxidation of CH_4 exposed to a Ni catalyst on an Al_2O_3/SiO_2 support and an Ar or Ar/O_2 APPJ, using time-resolved DRIFTS. The authors found that treatment with Ar plasma resulted in the formation of surface-bound CO, which was oxidised to CO_2 upon admixture of O_2 to the plasma. These results indicate that the CO selectivity can be altered by adjusting the flow of O_2.[34] Gibson *et al.*[35] investigated CH_4 oxidation using a Pd/Al_2O_3 catalyst in a plasma. From *in situ* monitoring of the X-ray absorption fine structure (XAFS) the authors concluded that the catalyst did not undergo any significant structural changes during operation. Additionally, the temperature of the Pd nanoparticles was lower than needed to thermally activate the catalyst, indicating an alternative pathway for CH_4 activation.[35] Stere *et al.*[36] studied the oxidation of CH_4 in the plasma with a Pd/Al_2O_3 catalyst, using *in situ* DRIFTS analysis. The authors observed significant formation of formate species (HCOO) on the catalyst, which was correlated to CO_2 formation. They also suggested that CO and CO_2 formation occurs via different routes, due to their different formation profiles as a function of time.[36]

Besides experimental mechanistic studies, a good insight in the underlying (plasma and catalytic surface) chemistry for plasma-catalytic POX of CH_4 can also be obtained by numerical modelling. Existing kinetic models on plasma-induced POX of CH_4 have been developed for plasma-only processes, and thus do not incorporate any plasma-catalyst interactions. Nevertheless, these models still provide useful insight in the gas phase chemistry. Nozaki *et al.*[19] stated that in POX of CH_4, CH_3 mainly forms oxygenates, while other CH_x result in CO and CO_2 formation. They also modelled streamer formation in CH_4 to study its fragmentation pattern. Goujard *et al.*[9] simulated POX of CH_4 at 5 °C and 300 °C. Plasma-induced dissociation of CH_4 in H and CH_3 was found to be the main mechanism for CH_4 activation at 5 °C, while at

300 °C, oxidation reactions became increasingly important, resulting in more CO, H_2, CO_2 and H_2O.[9] De Bie *et al.*[37] simulated POX of CH_4 in a DBD using a 1D fluid model and identified the dominant reaction pathways. Both De Bie *et al.*[37] and Goujard *et al.*[9] reported that CH_3 and O_2 recombine into CH_3OO, which was identified as a key species for oxygenate formation. On the other hand, Qian *et al*.[38] reported that CH_3OH is mainly formed via three-body recombination of CH_3 and OH, rather than via CH_3OO, based on 0D modelling.[38] An important issue for plasma-induced POX of CH_4 is deep oxidation to CO and CO_2, either due to oxidation of the oxygenates or dissociation of CH_4 to CH_2, CH or C, as is discussed in the abovementioned studies.[9,19,37]

While modelling POX of CH_4 in a plasma without catalyst gives useful insight in the gas phase chemistry, theoretical studies from thermal catalysis can provide a better understanding of the chemistry at the catalyst surface. Olivera *et al.*[39] estimated reaction enthalpies and activation barriers for POX of CH_4 on different transition metals (Ni, Pd, Pt and Au), using bond order conservation theory and found that CH_3OH formation is more likely to occur on the most noble metals. A similar conclusion was drawn by Yoo *et al*.[40] from microkinetic modelling of the thermal-catalytic POX of CH_4 on different transition metals. However, at the same time, activation of CH_4 is more difficult on the most noble metals.[39] Density functional theory (DFT) calculations by Xing *et al.*[41] showed that surface-bound O* can facilitate the activation of CH_4 on group Ib metals, but also lowers the barrier of the subsequent dehydrogenation steps, and therefore has both a promoting and inhibiting effect on POX of CH_4 towards oxygenates.[41] Baek *et al*.[42] performed microkinetic modelling on thermal POX of CH_4 to syngas and showed that if O*-assisted dehydrogenation pathways are considered, an additional local maximum in the turnover frequency (TOF) for CO_2 production can be observed in the region near Ag. Additionally, the TOFs of CO and H_2O also strongly increased in this region, yet the authors did not study oxygenate formation.[42]

Although the aforementioned theoretical studies provide useful knowledge on either the plasma or the catalyst surface chemistry, they are developed to simulate plasma-only or thermal-catalytic POX of CH_4, respectively. As a result, these studies do not incorporate any effects of plasma species on the surface chemistry. In this publication, we introduce a microkinetic model for POX of CH_4 by plasma catalysis, that incorporates the effects of plasma species, such as vibrationally excited molecules, radicals and stable intermediates, on the catalyst surface chemistry. Recently, similar models have provided valuable new insight in the plasma-catalytic synthesis of NH_3[43,44], non-oxidative coupling of CH_4[45] and CO_2 hydrogenation.[46]

Transition metals from group VIIIb are known to be good catalysts for thermal POX of CH_4 to syngas at high temperature.[8,47] We here investigate whether such transitions metals would be suitable catalysts for oxygenate production via low-temperature POX of CH_4 in the presence of reactive plasma species. From these catalysts, we choose Pt(111) as this is among the most noble transition metals in group VIIIb and can thus be expected to be the more suitable catalyst for oxygenate formation.[39] Note that it is described in literature that plasma methods for catalyst preparation, e.g. catalyst reduction by plasma, can easily generate the (111) facet.[48] Additionally, Pt has been fairly well studied in thermal catalysis for syngas formation through POX of CH_4 at high temperature by both microkinetic modelling[49–52] and DFT studies.[53,54] Thus, the DFT data required by the model is accessible in literature and the availability of other microkinetic modelling studies allows us to compare our results to those of existing studies.

2. Methods

We constructed a mean field microkinetic model to simulate POX of CH_4 on Pt(111).[45] For every surface species the time-evolution of the fractional coverage is described with a balance equation, based on the different gain and loss terms:

$$\frac{\partial \theta_x}{\partial t} = \sum_{i,\,gain} c_{x,i} r_i - \sum_{i,loss} c_{x,i} r_i \qquad (1)$$

Where θ_x is the fractional coverage of species x, $c_{x,i}$ is the stoichiometric coefficient for species x in the gain and loss reactions i and r_i are the rates of said reactions. These rates are calculated as the difference between the rates of the forward and reverse reactions:

$$r_i = k_{i,f} \prod_{x_f} (a_{x_f})^{c_{x_f,i}} - k_{i,r} \prod_{x_r} (a_{x_r})^{c_{x_r,i}} \qquad (2)$$

Where $k_{i,f}$ and $k_{i,r}$ are the rate constants of the forward and reverse reactions, respectively, and a_{xf} and a_{xr} are the activities of the reactant species x_f and the product species x_r, respectively. The activities are assumed equal to the fractional coverages for surface species and to the partial pressures (in bar) for gas phase species. The rate constants are calculated using transition state theory:

$$k = \frac{k_b T}{h} \exp\left(-\frac{\Delta G^{\ddagger}}{RT}\right) = \frac{k_b T}{h} \exp\left(-\frac{\Delta H^{\ddagger}}{RT}\right) \exp\left(\frac{\Delta S^{\ddagger}}{R}\right) \qquad (3)$$

Where k_b is the Boltzmann constant, T is the temperature, h is the Planck constant, R is the ideal gas constant and $\Delta G^{\ddagger}$, $\Delta H^{\ddagger}$ and $\Delta S^{\ddagger}$ are the Gibbs free energy, enthalpy and entropy of

activation, respectively. We calculate the entropy differences based on the translational entropy, as this typically has the largest contribution to the total entropy.[55] The translational entropy of a gas species is calculated as:[56]

$$S_{trans}(T) = R\ ln\left(\frac{k_b T\left(2\pi \mathrm{m k_b} T\right)^{3/2}}{p_{ref}\qquad h^3} e^{5/2}\right) \tag{4}$$

Where S_{trans} is the translational entropy, m is the mass of the gas species and p_{ref} is the reference pressure (10^5 Pa). Gas phase species are assumed to lose all their translational entropy upon adsorption onto the surface. Thus, the reaction entropy ΔS is equal to $-S_{trans}$ for adsorption processes and Eley-Rideal reactions. For dissociative adsorption and Eley-Rideal reactions, the transition state is assumed to have lost all its translational entropy, hence $\Delta S^{\ddagger}_{ads}$ is equal to $-S_{trans}$. For molecular and radical adsorption, on the other hand, the transition state is considered a 2D gas and $\Delta S^{\ddagger}_{ads}$ is considered equal to $-1/3 S_{trans}$ for these processes.[56] For the corresponding molecular and radical desorption processes, the Gibbs free energy of activation can become negative at higher temperatures, due to the higher entropy in the transition state. In such case, the Gibbs free energy of activation $\Delta G^{\ddagger}_{des}$ is set to zero and the rate constants are calculated as:

$$k_{des} = \frac{k_b T}{h} \tag{5}$$

$$k_{ads} = \frac{k_{des}}{K_{eq,\,des}} \tag{6}$$

Where K_{eq} is the equilibrium constant:

$$K_{eq} = \exp\left(-\frac{\Delta G}{RT}\right) = \exp\left(-\frac{\Delta H}{RT}\right)\exp\left(\frac{\Delta S}{R}\right) \tag{7}$$

Where ΔG, is the Gibbs free energy of the reaction, ΔH is the reaction enthalpy and ΔS is the reaction entropy. Finally, ΔS and $\Delta S^{\ddagger}$ are considered equal to zero for Langmuir-Hinshelwood reactions.

A full list of all reactions included in the model alongside the thermodynamic data can be found in Table S1 of the Supporting Information (SI). The effect of vibrationally excited CH_4 and O_2 is implemented by lowering the enthalpy barriers of their respective dissociative adsorption reactions and the Eley-Rideal reactions between gaseous CH_4 and surface-bound OH* or O* (see Table S1 in the SI, reactions 14 and 15).[45] For a detailed description of how vibrational excitation is implemented in our model, we refer to section 2 of the SI.

We obtain steady state coverages, by solving the differential equations to $\left(\frac{\partial \theta_x}{\partial t} = 0\right)$ for all species, at a temperature of 500 K, a total pressure of 1 bar and zero conversion, unless noted otherwise. These steady state coverages can be inserted back into the rate equations to obtain steady state reaction rates. To compare the product formation and product distributions between different conditions, we calculate the steady state turnover frequencies (TOFs) and selectivities from the steady state reaction rates, as described in section 3 of the SI.

3. Results and discussion

In the following sections, we solve the model for various cases. We start by solving the model for the thermal case, without including any plasma effects. These results will serve as the benchmark to evaluate the plasma effects. Subsequently, we modify the model to include either vibrational excitation or plasma-generated radicals and stable intermediates and we compare these results to the thermal case. In order to make this comparison possible, all simulations are performed at a temperature of 500 K and a total pressure of 1 bar, unless noted otherwise. We choose these conditions as they are representative for a DBD plasma. In our simulations, we use a reactant gas mixture of CH_4/O_2 (70/30), as the radical partial pressures used in our model are based on radical densities calculated by De Bie *et al.*,[37] for this gas mixture. This CH_4/O_2 ratio is close to the stoichiometric ratio of 2/1 for POX to CH_3OH. Note that this work focusses on the effect of the plasma species on the surface chemistry. In reality, molecules and radicals formed at the catalyst surface can desorb back to the gas phase and in turn influence the plasma chemistry. The influence of the surface reactions on the plasma composition is beyond the scope of this study but would be an interesting follow-up work.

3.1. Thermal catalysis

As discussed in the introduction, the thermal-catalytic POX of CH_4 on Pt has been mainly investigated for the production of syngas at high temperatures (800 – 1300 K).[49–52,57,58] Only a few studies have investigated potential pathways for oxygenate formation via POX of CH_4 on Pt.[39,40,53] We start by solving the model for the thermal case to reveal the most important reaction pathways for POX of CH_4 on a Pt(111) surface at steady state. The overall pathways for the main products are shown in Figure 1a. Gaseous CH_4 dissociatively adsorbs onto the surface, forming CH_3* and H*. CH_3* is further dehydrogenated to CH_2*, which in turn forms CH*. We find that the breaking of the C-H bonds in all three steps occurs through interaction with empty surface sites, rather than with OH* or O*. Most of the CH* (90.5%) is oxidised to CHO* and subsequently decomposes to form CO*, which desorbs from the surface. A smaller

fraction of CH* (9.4%) first undergoes dehydrogenation, after which the formed C* is oxidised into CO* as well. Dissociative adsorption of O_2 results in formation of surface O*. Most of the O* (79.0%) forms OH* through reaction with H* that originates from the dehydrogenation of CH_x and CHO*, while the oxidation of CH* to CHO* is responsible for 18.0% of the total O* consumption. OH* reacts to form H_2O* through the reaction $2OH^* \rightarrow H_2O^* + O^*$, after which the formed H_2O* desorbs as a side product.

As mentioned before, we performed these calculations at 500 K, to provide a benchmark for plasma-catalytic POX of CH_4, which typically occurs at such temperature in DBD plasma, although we admit that this temperature is too low for thermal-catalytic POX of CH_4. Therefore, in the SI (section 4), we compare the reaction pathways at 500 K from Figure 1a with the pathways calculated at 1000 K (as more common in thermal-catalytic POX of CH_4) and results predicted by earlier microkinetic studies[50,52].

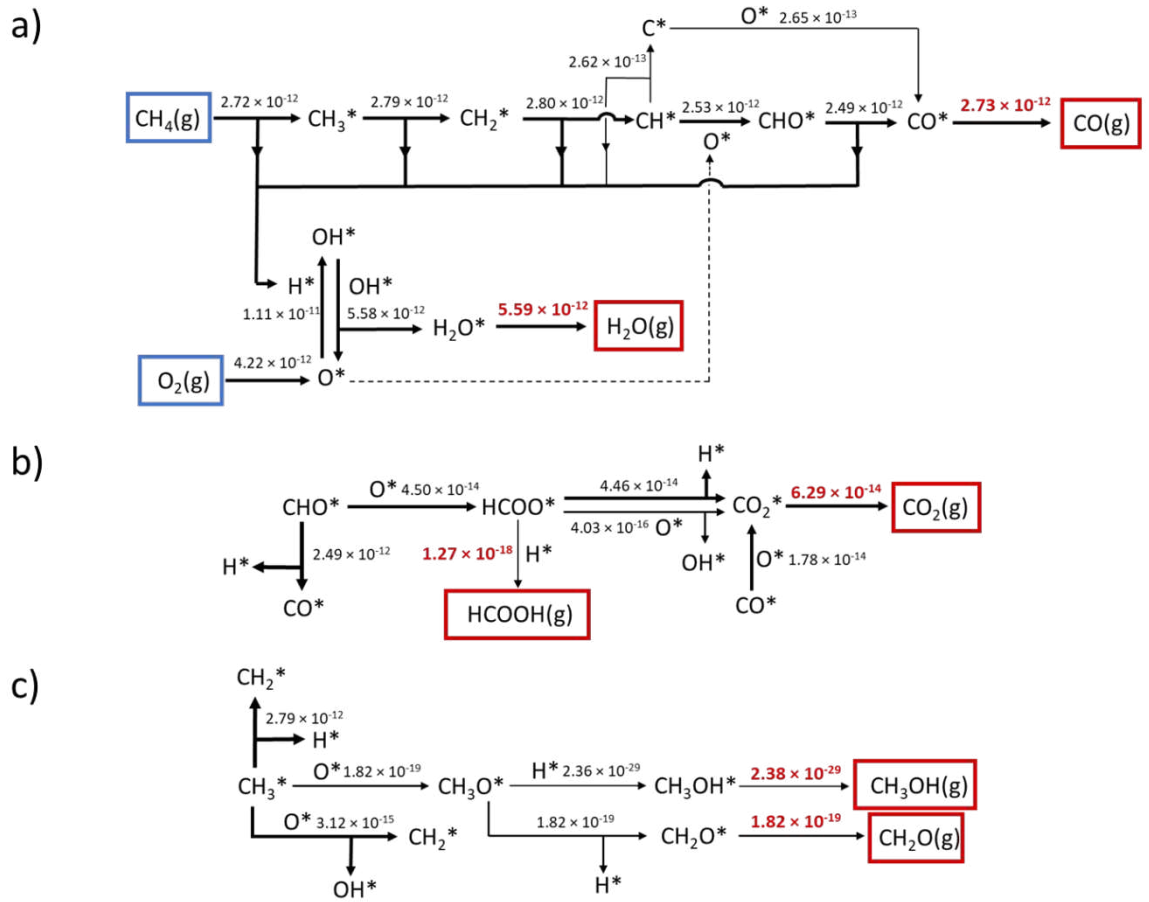

Figure 1. Most important reaction pathways at steady state for thermal-catalytic POX of CH_4 on Pt(111) using a CH_4/O_2 (70/30) gas mixture at 500 K and 1 bar. The values of the reaction TOFs in (s^{-1}) are displayed next to the arrows. The arrow thickness indicates the relative importance of a reaction within each separate scheme. A dotted arrow indicates the species is used as a second reactant in another reaction.

Figure 1b represents the pathways for the formation of CO_2 and HCOOH, as well as concurrent reactions. A relatively small amount (1.8%) of the CHO* formed in the main pathway, is oxidised to HCOO* as a side reaction. Only a minor amount (0.003%) of this HCOO* undergoes hydrogenation to HCOOH, while the majority is dehydrogenated to CO_2*, either by interaction with an empty surface site (99.1%) or O* (0.9%). Another important route for the formation of CO_2* is through oxidation of CO* that is formed in the main pathway. Still, about 71.0% of CO_2* formation occurs via dehydrogenation of HCOO* by empty sites, compared to 28.4% from oxidation of CO*. The rate of HCOOH formation in Figure 1 is about six order of magnitude lower compared to that of CO desorption, which indicates that the formation of HCOOH in practice does not occur. The rate of CO_2 desorption in Figure 1 is roughly a factor 40 lower than that of CO. However, experimental and DFT results by Chin *et al.*[59] indicate that CO oxidation to CO_2 is much faster than CH_4 dissociation on Pt clusters, and because of this, only trace amounts of CO can be present in the gas phase prior to O_2 depletion. Additionally, thermal equilibrium calculations show that CO_2 and H_2O are the thermodynamically favoured products at 500 K.[4,8] The reason that the rate for desorption of CO in Figure 1 is higher than that of CO_2 can, however, be attributed to the zero conversion conditions. Indeed, we find that the addition of even small amounts of CO (0.1-0.001%) to the gas mixture results in CO_2 becoming the main product, as CO is adsorbed and oxidised. A more in-depth discussion is provided in section 5 of the SI.

The pathways leading to the formation of CH_3OH and CH_2O are displayed in Figure 1c. These pathways branch off from the main reaction pathway at the CH_3* species, which can be oxidised by O* to form CH_3O*. The latter serves as a precursor for both CH_3OH and CH_2O. However, dehydrogenation of CH_3* by an empty surface site or a surface-bound O* is strongly favoured over CH_3O* formation, as indicated in Figure 1c. Indeed, the TOFs of dehydrogenation by empty sites or hydrogen abstraction by O* are seven and four orders of magnitude higher, respectively, than that of CH_3O* formation. The CH_3O* species can either be hydrogenated to CH_3OH or dehydrogenated to form CH_2O, the latter being strongly favoured (i.e., its rate is ten orders of magnitude higher). However, neither of these products are expected to be formed in significant amounts under these conditions, as their TOFs are several orders of magnitude lower than those of the main products, i.e., CO, CO_2 and H_2O. As mentioned earlier, this is also the case for HCOOH.

3.2. Plasma catalysis: effect of vibrational excitation

As discussed in the introduction, one of the challenges associated with POX of CH_4 is the activation of the strong C-H bond in CH_4.[7] Indeed, activation of the C-H bond has been identified as the sole kinetically relevant step for POX of CH_4 on Pt clusters, except for conditions close to O_2 depletion, where O_2 activation becomes rate-limiting.[60] Vibrational excitation of CH_4 is known to enhance its dissociative adsorption onto transition metal surfaces.[61] Thus, plasma-induced vibrational excitation can be expected to facilitate POX of CH_4 on these surfaces. In the following sections we investigate the impact of vibrational excitation on the TOFs and product selectivities of POX of CH_4 on Pt(111), and we discuss the associated kinetic and mechanistic changes. We implement the effect of plasma-induced vibrational excitation by lowering the barriers of CH_4 and O_2 activation, as discussed in section 2 of the SI. We simultaneously vary the vibrational temperatures of CH_4 and O_2 between 500 and 1500 K and assume both vibrational temperatures to have the same value. Chen *et al.*[62] measured the vibrational temperature in a CH_4/N_2/He DBD plasma at 60 Torr based on the $\nu = 1$ peak of N_2 and observed a maximal vibrational temperature of 1350 K. We here choose an upper limit of 1500 K, which is still in the uncertainty range of the results from Chen *et al.*[62] We choose this value to be an upper limit since the vibrational temperature measured by Chen *et al.* was based on the $\nu = 1$ peak of N_2 and the vibrational temperature of CH_4 is likely to be lower. As a comparison, Butterworth *et al*.[63] studied the vibrational excitation of CH_4 in low pressure pulsed microwave plasma and found that the vibrational and gas temperatures equilibrate around 900 K. In any case, varying the vibrational temperature in this wide range is interesting from a theoretical point of view as well.

3.2.1. Effect of vibrational excitation on the TOFs

Figure 2 illustrates the influence of vibrational excitation on the total TOF of CH_4 dissociation for a variable O_2 content (1-99%), as well as the separate TOFs of the two main CH_4 dissociation reactions. As can be seen in the right panel of Figure 2, the TOF of CH_4 dissociation increases by several orders of magnitude, i.e. about 4 orders of magnitude at 30% O_2, upon a rise in vibrational temperature from 500 to 1500 K. Additionally, the CH_4 dissociation TOF also rises upon lower O_2 content due to the corresponding increase in the partial pressure of CH_4. Below a vibrational temperature of 1000 K, the highest CH_4 dissociation TOFs are restricted to low O_2 content. Yet, above 1000 K the highest TOFs can be found in a region that is more spread out over the different O_2 fractions. This can be linked to a change in the main mechanism of CH_4 dissociation around 1000 K. The TOFs of the main mechanisms of CH_4

dissociation can be seen in the left panels of Figure 2. At vibrational temperatures below 1000 K, the main mechanism for CH_4 dissociation is the dissociative adsorption on empty surface sites, while above 1000 K the dissociation of CH_4 occurs mostly through an Eley-Rideal reaction with pre-adsorbed O* ($CH_4(g) + O^* \rightarrow CH_3^* + OH^*$). The change in mechanism follows from a stronger rise in the rate constant of the O*-assisted CH_4 dissociation, compared to dissociative adsorption on empty sites. This is a direct result of the higher reaction barrier and Fridman-Macheret α parameter (see SI, section 2) of the O*-assisted reaction (1.28 eV and 0.48 eV, resp.) compared to that on empty sites (0.63 eV and 0.41 eV, resp.). When comparing the TOFs of both reactions, we find that the O*-assisted mechanism depends less on the O_2 content in the gas mixture. This is because the O* coverage varies very little with O_2 content or vibrational temperature and remains above 99.5% in the investigated range, while the fraction of free sites mainly changes with O_2 content and drops from 5.3×10^{-5} to 3.7×10^{-6}, as the O_2 content rises from 1 to 99%. As the O*-assisted mechanism depends less on the fraction of free sites, i.e., it requires only one free site per molecule of CH_4, it also varies less with O_2 content. The fractional coverages of the 14 most abundant surface species, as well as the fraction of free sites, can be found in Figure S3 in the SI.

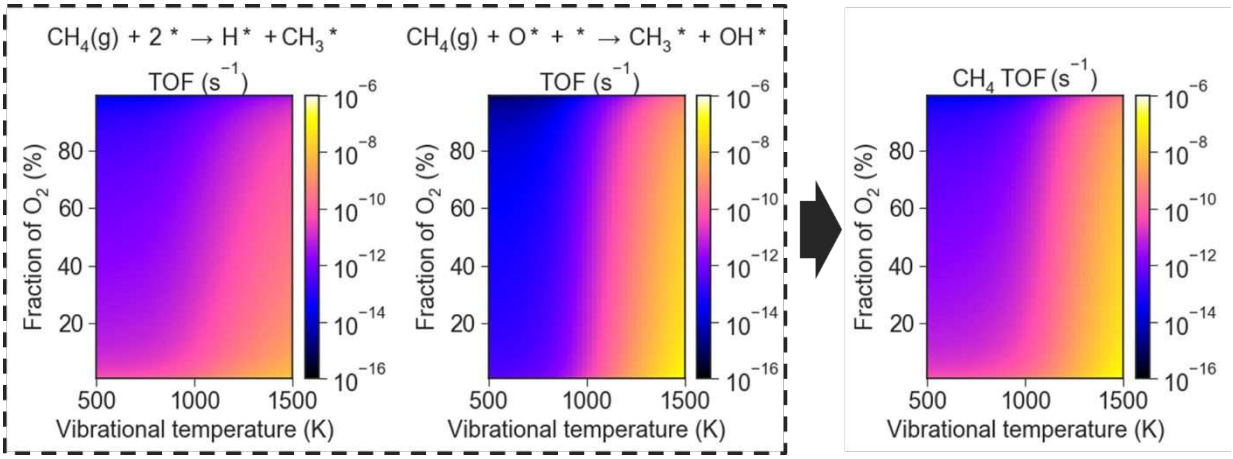

Figure 2. Influence of the vibrational temperature and O_2 content on the TOFs of the two main reactions for CH_4 dissociation (left panels) and on the total TOF of CH_4 dissociation (right panel), both in (s^{-1}). Calculated at steady state for a CH_4/O_2 mixture at a pressure of 1 bar and a surface temperature of 500 K. For convenience the same scale is used for the three graphs in this figure.

Our results indicate that plasma-induced vibrational excitation shows good potential for improving the TOFs of POX of CH_4 at low temperature (500 K). The effect of vibrational excitation on the product selectivities is discussed in the next section. Additionally, our results suggest that vibrational excitation can decrease the dependency of the TOFs on the O_2 content in the gas phase for relevant O_2 fractions (1-99%) by facilitating the O*-assisted dissociation of CH_4. As a result, high TOFs becomes feasible even at higher O_2 fractions.

3.2.2. Effect of vibrational excitation on the selectivities

In the previous section we showed that vibrational excitation can enhance the TOF of CH_4 dissociation. In this section we investigate whether vibrational excitation can affect the selectivities of the products. In Figure 3 we illustrate how the selectivities of the oxygenates, CO_x and ethane (CH_3CH_3) change when varying the vibrational temperature from 500 to 1500 K for a gas mixture with variable O_2 content, i.e. 1-99% O_2. Figure 3a), Figure 3b) and Figure 3c) display the selectivities of CH_3OH, HCOOH and CH_3CH_3, respectively, which show a similar trend. The selectivities of these products rise strongly when increasing the vibrational temperature from 500 to 1500 K, i.e. by a factor 10^4-10^5 at 33% O_2. However, these selectivities are less dependent on the O_2 content in most of the investigated range and only show a strong decrease at high O_2 fractions. Figure 3d) and Figure 3e) display the selectivities of CH_2O and CO_2, respectively. The selectivities of both products increase only slightly with a rising vibrational temperature and instead depend stronger on the O_2 content in the gas mixture, with a higher fraction of O_2 resulting in higher selectivities towards these products. The selectivity of CO, shown in Figure 3f), changes little under the investigated conditions, but drops slightly with rising O_2 fraction or vibrational temperature. As a result, CO remains the main product under the investigated conditions.

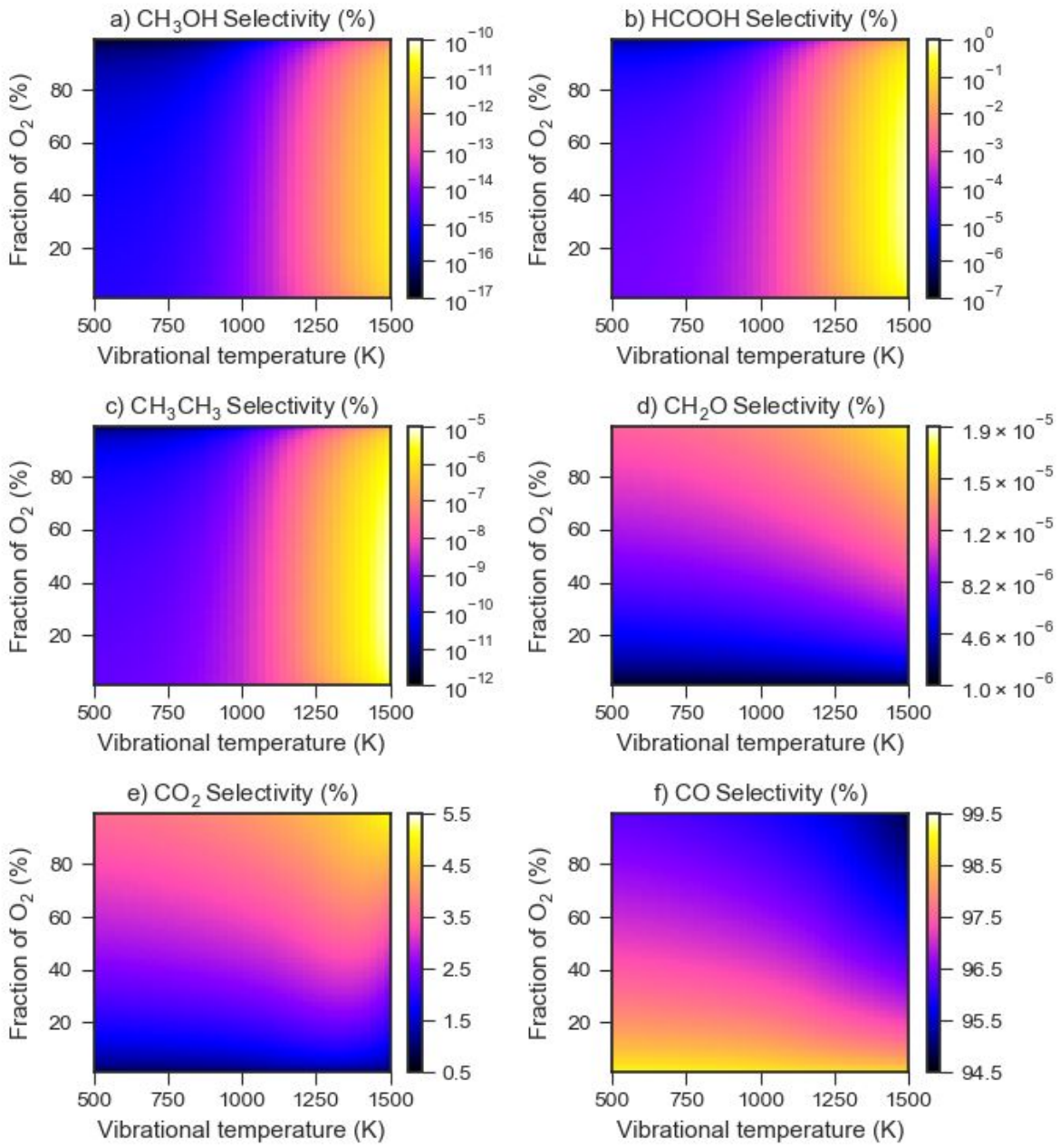

Figure 3. Influence of the vibrational temperature and O_2 content on the selectivities of oxygenates, CO_x and CH_3CH_3. Calculated at steady state for a CH_4/O_2 mixture at a pressure of 1 bar and a surface temperature of 500 K. Note that logarithmic scaling is used for CH_3OH, HCOOH and CH_3CH_3, while linear scaling is used for CH_2O, CO_2 and CO.

The similar trend for the selectivities of CH_3OH, HCOOH and CH_3CH_3, which strongly increase with rising vibrational temperature, can be explained by the enhanced dissociation of CH_4. Vibrational excitation facilitates CH_4 dissociation, which enhances the formation of CH_x* and H*. Therefore, as the vibrational temperature rises from 500 to 1500 K, the fractional coverages of these species increase, by about a factor 10^3-10^5 at 30% O_2 (see Figure S3 in the SI). Higher H* coverages enhance the hydrogenation of CH_3O* and HCOO* to CH_3OH and HCOOH, respectively, resulting in higher selectivities towards these products upon higher

vibrational temperature. Similarly, higher surface coverages of CH_x* enhance their coupling to form C_2-hydrocarbons. In Figure 3, we only show the selectivity of CH_3CH_3, but the selectivities of CH_2CH_2 and CHCH show a similar trend and can be found in Figure S4 in the SI. While the formation of CH_x* and H* is also enhanced at high CH_4 content and thus low O_2 fractions in the gas mixture, this trend is not observed as strongly in the selectivities of CH_3OH, HCOOH and C_2-hydrocarbons. This is because lower O_2 fractions also result in higher fractions of free sites, which promote the dehydrogenation of CH_x* and CO formation according to the pathways in Figure 1a. While vibrational excitation shows potential for improving the selectivities towards CH_3OH, HCOOH and C_2-hydrocarbons, these selectivities remain low under the investigated conditions, i.e. below 1.8×10^{-13}, 9.4×10^{-8}, 3.7×10^{-22} and 6.8×10^{-12} for CH_3OH, CH_3CH_3, CH_2CH_2 and CHCH, respectively. This indicates that the effect of vibrational excitation alone is not enough to make the formation of CH_3OH or C_2-hydrocarbons feasible on Pt(111). On the other hand, the selectivity towards HCOOH reaches a maximum of 0.77%, indicating that the formation of detectable amounts of HCOOH might be possible at high vibrational temperature.

As shown in Figure 3, the selectivities of CH_2O and CO_2 are not affected much by vibrational excitation and are instead more strongly dependent on the O_2 content in the gas mixture. Both products show increased selectivities at higher O_2 content, which is a result of the lower availability of free surface sites. As less free sites are available, a slightly lower fraction of CH_3* and CHO* can be dehydrogenated by empty sites. Instead, relatively more CH_3* and CHO* will bind to O*, forming CH_3O* and HCOO*, respectively. As can be seen from the pathways displayed in Figure 1, the latter two species are precursors to CH_2O and CO_2, respectively. While the selectivities towards both products thus increase upon higher O_2 fraction, they vary relatively little under the investigated conditions, i.e. from 1.2×10^{-8} to 1.7×10^{-7} and from 0.89% to 5.1% for CH_2O and CO_2, respectively. Consequently, the selectivity towards CH_2O remains too low for its formation to become feasible on Pt(111), when only considering vibrational excitation. We find that the coupling of CH_3* and O* to CH_3O* is a bottleneck for the formation of CH_2O and CH_3OH, as CH_3O* is a precursor to both these products. This reaction is strongly disfavoured on Pt(111), due to its high activation barrier (2.04 eV), while the barriers for CH_3* dehydrogenation by either an empty surface site or O* are lower (0.83 and 1.62 eV, resp.).[53]

In summary, our results show that plasma-induced vibrational excitation increases the CH_4 dissociation TOF in its POX. This supports the possibility of plasma catalysis to facilitate POX

of CH_4 on transition metals, like Pt, at lower temperatures than those required in traditional thermal catalysis. Additionally, we find that vibrational excitation increases the selectivities of CH_3OH, HCOOH and C_2 hydrocarbons. The lower activation barrier of CH_4 dissociation improves the formation of H* and CH_x* species at the catalyst surface, which enhances hydrogenation of CH_3O* and HCOO* and coupling of CH_x. However, we find that the selectivities towards oxygenates and C_2 hydrocarbons remain low on Pt(111), as C-H bond breaking of the surface-bound intermediates is too strongly favoured on this catalyst and the effect of vibrational excitation alone cannot counteract this.

3.3. Plasma catalysis: effect of radicals and stable intermediates

Radicals and stable intermediates formed in the plasma are implemented in the model by setting a non-zero partial pressure for these species. The base case assumes partial pressures based on species densities calculated by De Bie *et al.*,[37] for a DBD plasma at a CH_4/O_2 (70/30) inlet gas mixture. These species densities are converted to partial pressures using the ideal gas law and normalised to a total pressure of 1 bar. The resulting partial pressures are listed in Table 1. To study the impact of different species on the surface chemistry, their partial pressures are varied in a wide range. Ions are not considered in our model as they generally have lower densities compared to the radicals, indicating that they play only a minor role in the plasma chemistry.[37] Moreover, thermodynamic data for adsorption of ions from the gas phase is not readily available. However, in practice ions can also adsorb and react on the surface. For example, O_2 can be transformed into O_2^- by electron attachment in plasma. Following adsorption, O_2^-* can react with H_2O* to form OOH* and OH^-*.[64] While this reaction is thus not considered in our model, we do account for the formation of OOH* through adsorption from the plasma.

We study the effect of the plasma species listed in Table 1, in the absence of any vibrationally excited species, to examine both effects separately. Furthermore, we find that if both effects are included in the model, the impact of vibrational excitation on the product TOFs is negligible. This is illustrated in Figure S5 of the SI. This indicates that for plasma catalysis with DBD plasmas, the surface chemistry is mainly governed by the plasma radicals. Similar conclusions were drawn by Engelmann *et al.*[45] for plasma-catalytic non-oxidative coupling of CH_4.

Table 1: The partial pressures implemented in the model for the base case, i.e., CH_4/O_2 (70/30) inlet gas mixture. Based on species densities from De Bie et al.[37]

Reactants	Partial pressure (bar)	Radicals	Partial pressure (bar)
O_2	0.3	C	1.54×10^{-11}
CH_4	0.7	CH	1.02×10^{-13}
Stable intermediates	Partial pressure (bar)	CH_2	2.32×10^{-11}
CO	6.91×10^{-7}	CH_3	3.17×10^{-11}
CH_3OH	2.25×10^{-7}	O	2.09×10^{-7}
H_2	3.25×10^{-6}	H	2.72×10^{-10}
CH_3CH_3	2.34×10^{-7}	OH	8.96×10^{-9}
CH_2CH_2	5.07×10^{-7}	OOH	2.62×10^{-6}
CHCH	7.90×10^{-9}	CHO	4.62×10^{-13}
H_2O	1.30×10^{-6}	CH_3OO	3.25×10^{-6}
CO_2	5.85×10^{-7}	CH_3O	9.17×10^{-8}
CH_2O	1.98×10^{-6}		
HCOOH[a]	1.98×10^{-6}		

a) This partial pressure was set equal to that of CH_2O, as HCOOH is not included by De Bie *et al*.

3.3.1. Most important reaction pathways in the presence of plasma species

Figure 4 illustrates the most important steady state reaction pathways on a Pt(111) surface exposed to a CH_4/O_2 (70/30) plasma, i.e. including plasma-generated radicals and intermediates. The most important surface reactions, in terms of reaction rate, are adsorption of O radicals and subsequent associative desorption of the surface-bound O* to form O_2. Approximately 96.7% of O* is formed via adsorption of O radicals from the plasma and 85.6% of O* desorbs as O_2 into the gas phase, while the rest is used in oxidation processes at the surface.

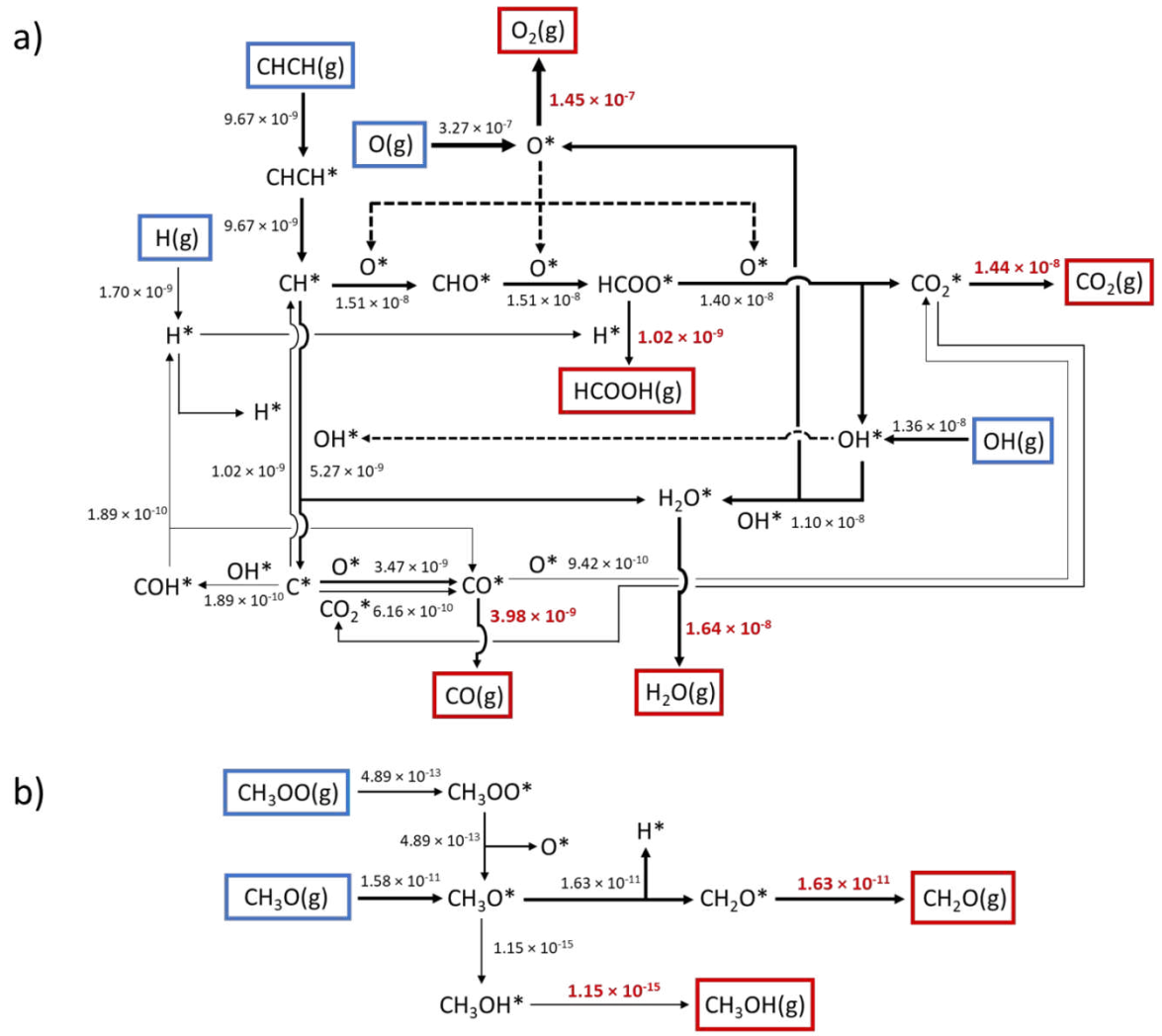

Figure 4. Most important reaction pathways at steady state for POX of CH_4 on a Pt(111) surface exposed to a CH_4/O_2 (70/30) DBD plasma at 500 K and 1 bar. The values of the reaction rates in (s^{-1}) are displayed next to the arrows. The arrow thickness indicates the relative importance of that reaction within each separate scheme. A dotted arrow indicates the species is used as a second reactant in another reaction.

The main carbon pathway starts from adsorption and subsequent dissociation of CHCH to CH*. The latter preferentially (74.2%) undergoes oxidation to CHO*, which in turn binds with O* to form HCOO*. Most of the HCOO* (92.4%) undergoes hydrogen abstraction by O* to form CO_2* and OH*, while 6.8% is hydrogenated to HCOOH. About 50.6% of the surface-bound OH* is formed from reaction between HCOO* and O*, while the remaining 49.4% is adsorbed from the plasma. Most of the OH* (80.0%) forms H_2O* and O* via a disproportionation reaction, while 19.1% reacts with CH* to form H_2O* and C*. H_2O* desorbs from the surface as a product. Surface-bound C* can either be oxidised to CO* (65.5%), undergo hydrogenation to again form CH* (19.3%), react with CO_2* to form two CO* molecules (11.6%) or bind to OH* to form COH* (3.6%). The latter decomposes into CO* and H*, forming about 9.2% of the surface-bound H*, though most H* (82.7%) is formed by direct adsorption from the plasma.

H* is mainly consumed in the hydrogenation of C* (49.8%) or the formation of HCOOH (49.7%). As discussed above, various routes lead to the formation of CO*. Most of the CO* (80.9%) desorbs from the surface as a product, while a smaller amount is oxidised to CO_2* (19.1%). Thus, our results show that any CO* that reacts further is not hydrogenated to oxygenates, but instead further oxidised to CO_2. The formation of oxygenates therefore occurs via another route than that of CO. While our results show that some CO_2 is formed via oxidation of CO*, we do not find this to be the main pathway for CO_2 formation. Instead, we find that CO_2 is mainly formed from HCOO* in a separate pathway. Interestingly, DRIFTS results by Stere *et al*.[36] indicate that in the plasma-catalytic oxidation of CH_4 on a Pd/Al_2O_3 catalyst, CO_2 formation also occurs via HCOO*. As Pt and Pd are part of the same group in the periodic table, similarities in their surface chemistry can indeed be expected.

Note that H_2O is formed as a major product. This might be troublesome, as the presence of H_2O vapor in a DBD plasma can alter the discharge behaviour, resulting in more, but less intense micro-discharges.[65] H_2O addition can also cause destabilisation of the discharge, and plasma chemistry calculations revealed a drop of approximately 40% in the maximum electron density upon increasing the water content from 0 to 8% in DBD plasma.[66] Additionally, a higher H_2O concentration results in a loss of electron energy due to H_2O rotational and vibrational excitation, as is discussed in literature for He/H_2O and Ar/H_2O plasmas.[65,67] The presence of H_2O in plasma also causes quenching of the vibrational levels of CO_2, which results in less CO_2 dissociation.[68] This might lead to a higher net production of CO_2. Moreover, the presence of H_2O might also result in additional CO_2 formation in the plasma through the water-gas shift.[69] This is in line with plasma chemical kinetics simulations and experiments, which revealed that H_2O addition to a CO_2 DBD plasma causes a drop in CO_2 conversion, and the detailed chemical kinetics scheme explaining this behaviour was presented in ref. [66]. Furthermore, this paper also explained the underlying chemistry why oxygenates formation was prohibited in this case. Therefore, it can be beneficial to remove H_2O from the gas phase through condensation by cooling of the reactor wall. In addition, this also removes condensable oxygenates from the gas phase and limits their further oxidation.[69,70]

Figure 4b represents the main reaction pathways for the formation of CH_3OH and CH_2O. As in the thermal case (see Figure 1), CH_3O* is a key species in the formation of both CH_3OH and CH_2O. Yet, in the thermal case, the formation of this species occurs on the catalyst surface, via O* addition to CH_3*, while Pt strongly favours CH_3* dehydrogenation instead. In the plasma case, on the other hand, CH_3O is formed in the plasma and subsequently adsorbs on the catalyst

surface. As is illustrated in Figure 4b for the plasma case, CH_3O* is either directly adsorbed from the gas phase (97.0%) or formed from adsorption of CH_3OO radicals and subsequent cleavage of the O-O bond (3.0%). The formed CH_3O* preferentially undergoes dehydrogenation to CH_2O (> 99.9%), while only a minor fraction is hydrogenated to form CH_3OH (0.007%).

In the presence of radicals, the reaction rates have generally increased compared to the thermal case. The TOF of CO and CO_2 have increased by about three and five orders in magnitude, respectively, compared to the thermal case. We find that CO_x are still the main products for the plasma case, with selectivities of 20.5% and 74.4% for CO and CO_2, respectively. However, the selectivities and TOFs of the oxygenates have strongly improved compared to the thermal case. The calculated selectivities of CH_3OH, CH_2O and HCOOH now reach 5.9×10^{-8}, 0.084% and 5.3%, respectively, which corresponds to a rise by about ten, four and five orders of magnitude, respectively. Although CH_3OH formation still does not seem to be feasible on Pt under these conditions, a reasonable amount of HCOOH is now formed on the surface. The combination of a catalyst with plasma radicals thus shows potential for enhanced oxygenate selectivities. Additionally, tuning the partial pressures of the radicals in the plasma might further improve the formation of oxygenates. In the next section, we therefore show how different radicals affect the surface chemistry, fractional coverages and product TOFs.

3.3.2. The role of plasma species in the surface chemistry

As mentioned before, the reaction pathways discussed in the previous section are based on species densities calculated by De Bie *et al*.[37] (see Table 1), which are specific for the selected reaction conditions. In this section, we aim to gain additional understanding of how variations in the plasma composition might alter the surface chemistry by examining the influence of various plasma species on the product TOFs and surface coverages. For this purpose, we vary the partial pressures of either individual species or groups of species by a scaling factor, while keeping the partial pressures of the other species constant on the values reported in Table 1. The species HCOO and COOH are not included in the model by De Bie *et al*.[37] and are therefore not included in the simulations discussed below. However, a discussion of the effect of these species is included in the SI (see further).

Oxidising species

Figure 5 illustrates how the TOFs of CO_x, oxygenates and CH_3CH_3 are affected by a variation of the O partial pressure over six orders of magnitude. Next to the TOFs, the surface coverages

of the most abundant surface species are also displayed. A drop in the partial pressure of O radicals results in a sudden decline of the product TOFs, combined with a strong rise in the surface C* coverage. Although our model does not contain a mechanism for cokes formation, i.e. clustering of carbonaceous species, like e.g. C*, CH*, CHCH*, high surface coverage of these species indicates that coking is likely to occur. Coking reduces the amount of available catalytic sites on the surface and thus lowers the product TOFs. Most of the TOFs in Figure 5 eventually stabilise upon further lowering of the O partial pressure, as OH* becomes the main oxidising species at the surface. On the other hand, a high partial pressure of O is also disadvantageous, as O* competes with other species for free sites. If the O partial pressure is too high, O* will poison the surface, causing the TOFs to decline as well.

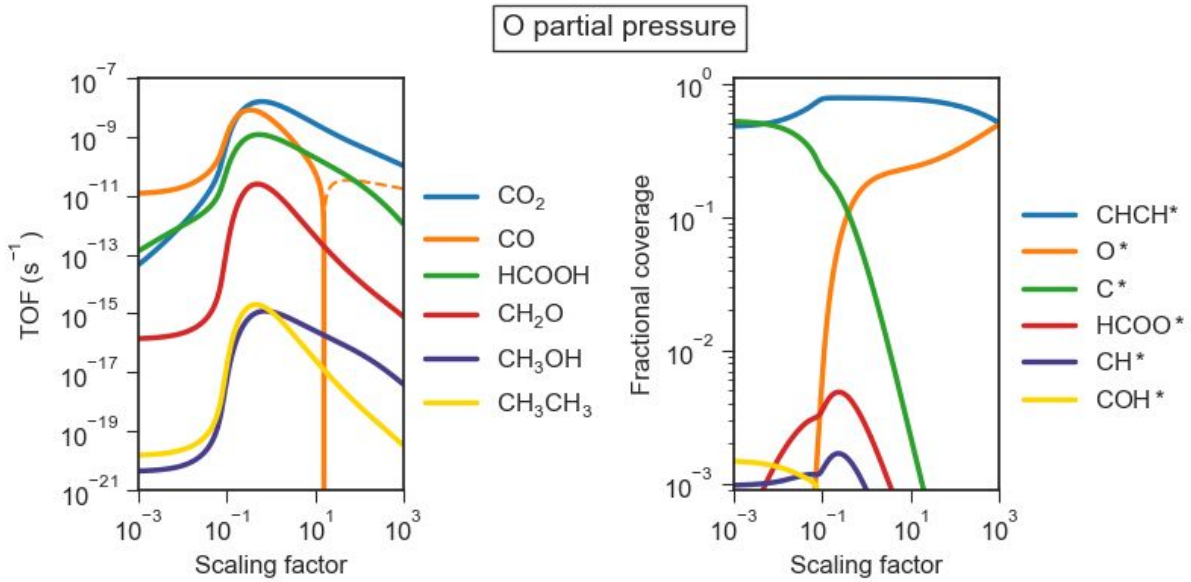

Figure 5. Influence of the O partial pressure on TOFs (left) and surface coverages (right). Dotted lines in the left graph indicate consumption, whereas full lines indicate production. Calculated for a temperature of 500 K and a total pressure of 1 bar. The species partial pressures used for these simulations are shown in Table 1, but the partial pressure of O is varied by the indicated scaling factor.

As can be seen in Figure 5, the O partial pressure can be used to tune the product selectivity between CO and CO_2. Low partial pressures of O radicals, which can be expected for plasmas with a high CH_4/O_2 ratio, favour the formation of CO. On the other hand, high O partial pressures, associated with low CH_4/O_2 ratios, give CO_2 as the main product. If the partial pressure of O is increased by about a factor 10, the faster oxidation of CO* results in net CO consumption, as plasma-produced CO adsorbs onto the surface and is oxidised to CO_2. Indeed, various experimental studies on plasma-catalytic POX of CH_4 report that transition metals (Ni,[29,31] Fe,[32] Pd[32] and Pt[30]) can catalyse the oxidation of CO to CO_2. Additionally, DRIFTS

and FTIR results by Zhang *et al.*[34] for plasma-catalytic CH_4 oxidation on Ni indicate that the selectivity of CO vs. CO_2 can be tailored by adjusting the introduction of O_2 to a plasma.

Next to O, we also examine the influence of the OH and OOH radicals as oxidising species (see section 9 and Figure S6 in the SI). Increasing the partial pressures of these species enhances the formation of OH* at the surface. The formed OH* promotes dehydrogenation of CH_x, which leads to more C* and thus favours CO formation. However, a further increase in the OH and OOH partial pressures results in a higher O* coverage, due to hydrogen abstraction from OH* by another OH*. This causes a drop in the surface coverage of most of the other surface species, which results in a decline of the product TOFs. Likewise, we present the effect of the HCOO and COOH radicals on the product TOFs and surface coverages in section 10 of the SI (Figures S7 and S8). We conclude that HCOO and COOH mainly result in additional formation of unwanted CO_2 and CO, and their formation in the plasma should therefore be limited.

In summary, oxidative species can reduce the coverage of carbonaceous species that could cause catalyst deactivation by coking. Yet, if the partial pressures of oxidative species are too high, the surface is poisoned with O* species instead. However, due to their reactive nature, plasma radicals might be able to react with surface-bound species, such as O*, via Eley-Rideal reactions with low to zero enthalpy barriers. In such case, high TOFs might be achieved even at high O* coverages. While our model does contain Eley-Rideal reactions, namely $CH_4(g) + OH^* \rightarrow CH_3^* + H_2O^*$ and $CH_4(g) + O^* \rightarrow CH_3^* + OH^*$, these reactions have higher enthalpy barriers (0.50 eV[71] and 1.28 eV[71], resp.) than what can be expected for similar reactions involving highly reactive radicals, rather than stable CH_4. In section 3.3.3 we therefore briefly illustrate the potential impact of Eley-Rideal reactions with plasma radicals for a range of enthalpy barriers. Further, our results show that tuning the amount of O radicals against the amount of C-containing species can be used to favour the production of CO over that of CO_2.

Carbonaceous species

The influence of the strongly dehydrogenated carbonaceous species (C, CH and CHCH) on the TOFs and surface coverages is shown in Figure 6. We include CHCH as well, as this is the most important species at the surface and the main source of surface carbon under the base conditions. As is shown in Figure 6, high partial pressures of these species lead to strong surface poisoning by CHCH* and thus a drop in the product TOFs. As mentioned before, these species can act as precursors for coking of the catalyst surface. We find that limiting the partial pressures of these carbonaceous species in the plasma has a beneficial effect on the TOFs of

most products. However, low partial pressures of these species lead to adsorption and oxidation of plasma-produced CO to CO_2, as can be seen in Figure 6. Because less carbonaceous species are available for reaction with O*, more O* reacts with surface-bound CO*. Simultaneously, less CO* can be formed through the pathways in Figure 4, as these pathways go via C*, leading to a net adsorption of plasma-produced CO. Furthermore, the simultaneous drop in the C, CH and CHCH partial pressures initially shows a beneficial effect on HCOOH formation, but scaling the partial pressures with a factor below 10^{-1} causes the TOF of HCOOH to decline. This results from the lower availability of CH* on the catalyst surface, as this species is required for HCOOH formation, according to the reaction pathways shown in Figure 4. At low partial pressures of the strongly dehydrogenated carbonaceous species, the HCOOH TOF in Figure 6 eventually stabilises, as CH_3 and CH_2 radicals become the main precursor species for the formation of CH* and HCOOH. In this regime, CH_2O becomes the most important oxygenate as its formation does not occur via CH*, but through CH_3O* and CH_3OO* instead.

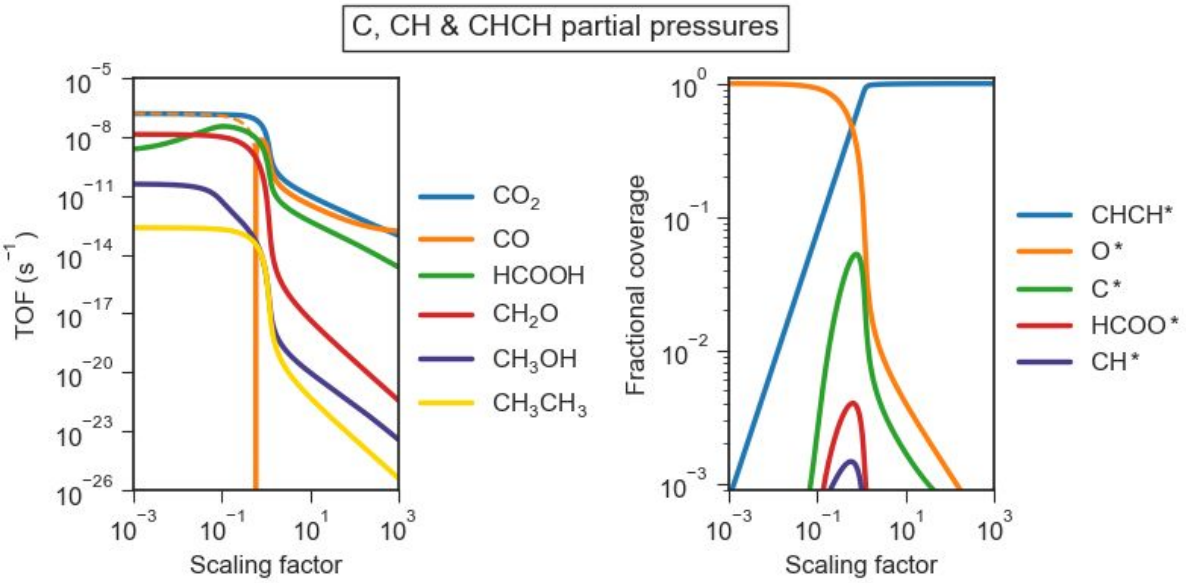

Figure 6. Influence of the C, CH and CHCH partial pressures on TOFs (left) and surface coverages (right). Dotted lines in the left graph indicate consumption, whereas full lines indicate production. Calculated for a temperature of 500 K and a total pressure of 1 bar. The species partial pressures used for these simulations are shown in Table 1, but the partial pressures of C, CH and CHCH are simultaneously varied by the indicated scaling factor.

Figure 7 displays the change in TOFs and fractional surface coverages, when increasing the partial pressures of CH_3 and CH_2 up to a factor 10^4. A higher partial pressure of these more hydrogenated carbonaceous species positively affects the TOFs, especially those of CH_3CH_3, HCOOH and CH_3OH. The effect on the TOF of CH_3CH_3 is straightforward, as a higher partial pressure of CH_3 improves the CH_3* coverages and its coupling towards CH_3CH_3. CH_3OH and HCOOH, on the other hand, benefit from the improved hydrogenation of CH_3O* and HCOO*,

respectively, because CH_3 and CH_2 provide the surface with more H* (due to catalytic dehydrogenation). Moreover, the formation of H* through dehydrogenation of CH_2* also forms CH*, which is an intermediate in the formation of HCOOH (see Figure 4). As can be seen in Figure 7, this results in HCOOH becoming the main carbon product (even slightly above CO_2) at around a scaling factor of 10^3. This shows that Pt is potentially a good catalyst for the plasma-catalytic HCOOH synthesis under plasma conditions with abundant CH_3 and CH_2 radicals (hence high CH_4/O_2 ratio), as it can readily dehydrogenate adsorbed CH_x* radicals to form CH*, while simultaneously forming the H* required in the hydrogenation of HCOO*, later on in the reaction path. However, as can be seen in Figure 7, enhancing the partial pressures of CH_3 and CH_2 by more than a factor 10^3 is no longer beneficial. The surface coverages indicate strong cokes formation past this point, resulting in a decline of most of the TOFs. Note that CH_3 and CH_2 themselves bind less strongly to the surface compared to CH and C,[71] and are less likely to act as coking precursors.

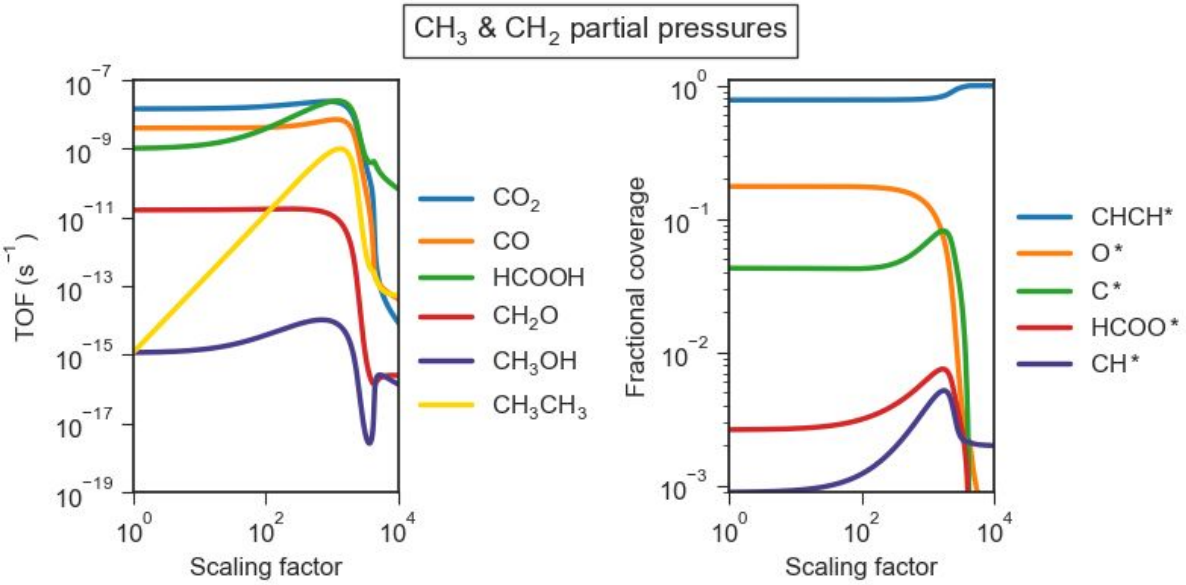

Figure 7. Influence of the CH_3 and CH_2 partial pressures on TOFs (left) and surface coverages (right). Calculated for a temperature of 500 K and a total pressure of 1 bar. The species partial pressures used in the simulations are shown in Table 1, but the partial pressures of CH_3 and CH_2 are simultaneously varied by the indicated scaling factor.

In summary, strongly dehydrogenated carbonaceous species are mainly precursors for cokes formation, and their partial pressures in the gas phase should ideally be kept low. These species also show some beneficial effect on HCOOH and CO formation at lower partial pressures. The more hydrogenated CH_2 and CH_3, generally show a more beneficial effect, enhancing the TOF of CH_3CH_3, HCOOH and CH_3OH at higher partial pressures, but also cause coking at very high partial pressures. The partial pressures of carbonaceous species can be expected to be higher for gas mixtures with high CH_4 content, but the ratio of less vs. more hydrogenated CH_x species

might be influenced by the CH_4 fragmentation pattern through electron impact dissociation in the plasma. Nozaki *et al.*[19] simulated streamer formation in CH_4 without catalyst and showed that the fragmentation pattern depends on the reduced electric field, with stronger reduced electric fields resulting in a larger fraction of more dehydrogenated CH_x species. Therefore, plasma characterised by weaker reduced electric fields can be expected to give less cokes formation. As discussed in the previous section, coking can also be counteracted by using high partial pressures of oxidising radicals, e.g. O, OH and OOH, and by tuning the partial pressures of oxidising species against those of carbonaceous species, the formation of either CO or CO_2 can be favoured. Moreover, the choice of the catalyst material can also be expected to play an important role in mitigating both coking and excessive oxidation, as different transition metals have different binding strengths for O and C. It is therefore essential in plasma catalysis to carefully tune the CH_4/O_2 ratio as function of the plasma conditions and the catalyst material.

Hydrogen radicals

Figure 8 illustrates the influence of the H radical partial pressure on the TOFs of CO_x, the oxygenates and CH_3CH_3, as well as the surface coverages of the most abundant surface species. A higher partial pressure of H strongly enhances HCOOH and CH_3OH formation. This is caused by the higher availability of H* on the catalyst surface, which improves the hydrogenation of CH_3O* and HCOO* to CH_3OH and HCOOH, respectively. Upon increasing the H partial pressure by about a factor 400, a strong rise in the TOFs of CH_3OH, CH_2O and CO_2 is observed. This is attributed to the improved hydrogenation of O* to H_2O*, which readily desorbs to make more free sites available. The fraction of free sites on the surface increases from about 10^{-10} to 10^{-6} in this region. This improves the adsorption of CH_3O, which can form both CH_3OH and CH_2O (see Figure 4b), and the adsorption of CO, which is oxidised to CO_2. At low H partial pressure, the TOFs in Figure 8 stabilise, as OH* now becomes the main source of H*. This results from coupling between OH* and C* followed by decomposition of the formed COH* to CO* and H*.

Given the favourable effect of the H radical on the formation of oxygenates, and especially CH_3OH, it is of interest to find a way to increase the partial pressure of H in the plasma. For its POX, CH_4 serves as the source of H in the plasma and increasing the CH_4 fraction in the feed gas might thus increase the partial pressure of H radicals. As discussed above, however, high CH_4/O_2 ratios might induce coking, due to the limited availability of oxidising species. Adding a H-containing co-reactant, such as H_2 or H_2O, might allow for more flexibility in maximizing the TOF of oxygenates, and especially CH_3OH.

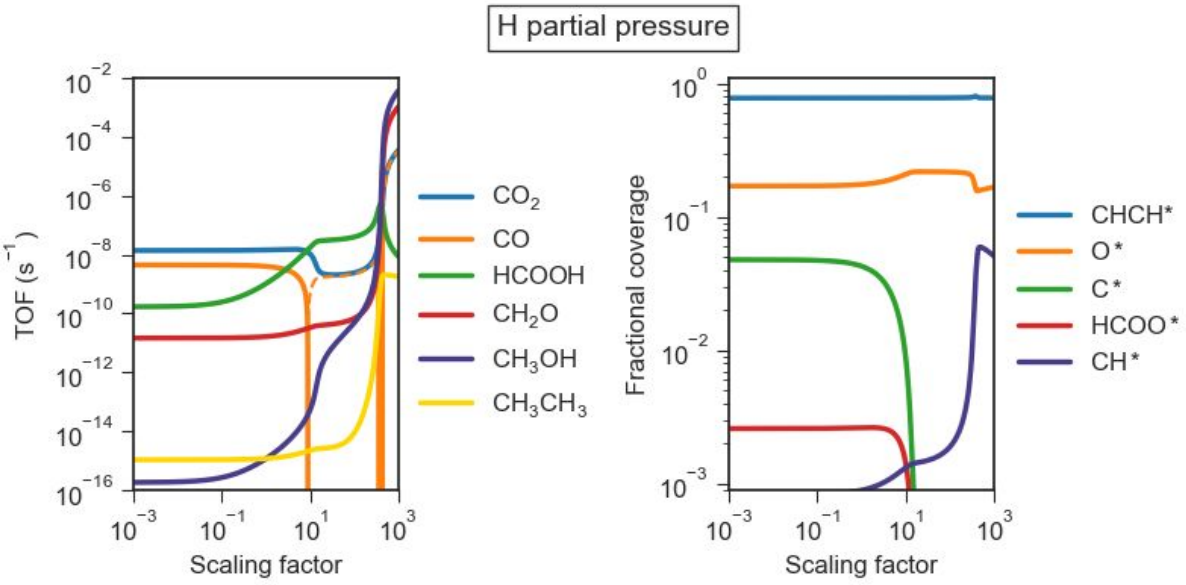

Figure 8. Influence of the H partial pressure on TOFs (left) and surface coverages (right). Dotted lines in the left graph indicate consumption, whereas full lines indicate production. Calculated for a temperature of 500 K and a total pressure of 1 bar. The species partial pressures used in the simulations are shown in Table 1, but the partial pressure of H is varied by the indicated scaling factor.

<u>CH_3O and CH_3OO radicals</u>

Modelling results by De Bie *et al.*[37] for plasma-only POX of CH_4 indicate that the CH_3O and CH_3OO radicals are important intermediates in the pathways leading to CH_3OH production in plasma. Our results show that for plasma catalysis these species also play an important role in the formation of CH_3OH and CH_2O at the catalyst surface, as indicated by the pathways in Figure 4b. We are therefore interested in the influence of these species on the catalyst surface chemistry and thus examine how a variation in their partial pressures affects the TOFs and fractional coverages at the catalyst surface. The results are shown in Figure 9.

As CH_3O and CH_3OO are precursors to both CH_3OH and CH_2O, the TOFs of these products strongly depend on the partial pressures of CH_3O and CH_3OO, while the TOFs of the other products are largely unaltered. Only at high partial pressures, where the adsorption and subsequent decomposition of CH_3O becomes important, the TOFs of the other products are also influenced, as can be seen in Figure 9. The decomposition of CH_3O* leads not only to the formation of CH_2O*, but also provides H*. The higher availability of H* improves HCOO* hydrogenation, so that CH_2O and HCOOH eventually become the main products (even above CO and CO_2). Moreover, the rise of the CH_3OH TOF also becomes much steeper in this region, illustrating the strong beneficial effect of both CH_3O* and H* on the CH_3OH formation. We also observe a shift in the surface coverages in Figure 9, as more C* is converted to CH*. The lower surface coverage of C* and preferred conversion of HCOO* to HCOOH at high CH_3O

and CH_3OO partial pressures, limit the formation of undesired CO and CO_2. We therefore find that CH_3O and CH_3OO can play an important role in enhancing the formation of oxygenates. Additionally, our results show that Pt is potentially a good catalyst for CH_2O synthesis, as CH_3O selectively decomposes to CH_2O on this catalyst. Moreover, it might be possible to vary the selectivity between CH_3OH or CH_2O by changing the catalyst material, as more noble transition metals have lower barriers for CH_3O hydrogenation and higher barriers for its dehydrogenation.[39]

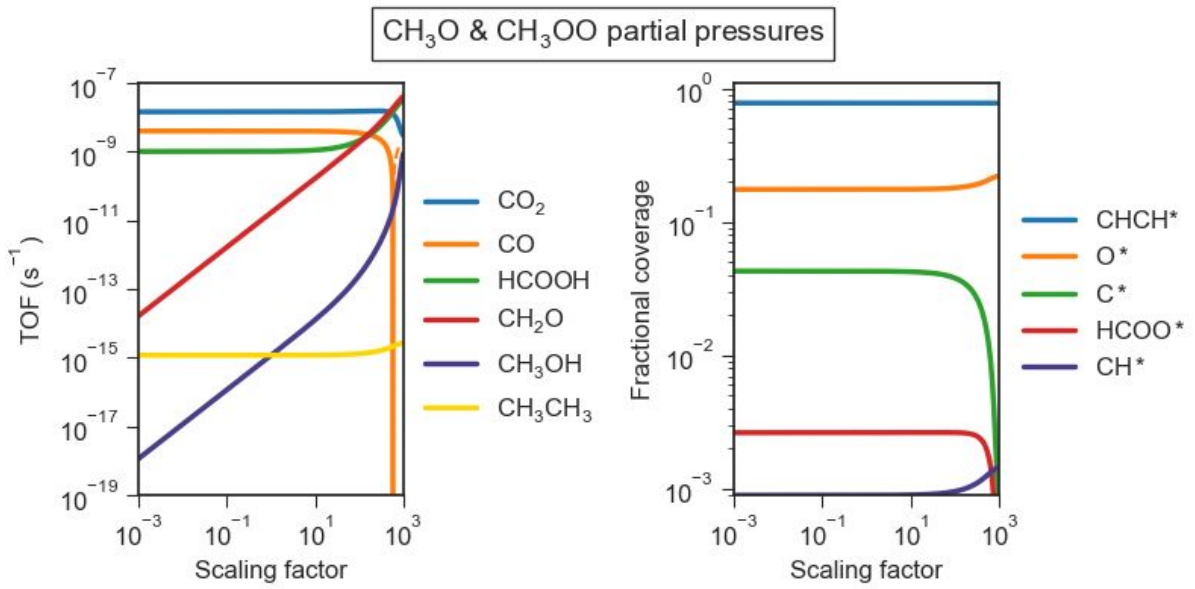

Figure 9. Influence of the CH_3O and CH_3OO partial pressures on TOFs (left) and surface coverages (right). Dotted lines in the left graph indicate consumption, whereas full lines indicate production. Calculated for a temperature of 500 K and a total pressure of 1 bar. The species partial pressures used in the simulations are shown in Table 1, but the partial pressures of CH_3O and CH_3OO are simultaneously varied by the indicated scaling factor.

Plasma-generated radicals and stable intermediates in general

In Figure 10, we illustrate how the TOFs and fractional coverages are affected by simultaneously lowering the partial pressures of all plasma-produced radicals and stable intermediates by a factor 10^{-6}. The product TOFs, especially those of CH_2O and CH_3OH, initially rise upon lowering the partial pressures of these plasma species, and CH_2O becomes the main product (clearly above CO and CO_2) below a scaling factor of 10^{-2}. Its TOF keeps rising upon lowering the partial pressures by a factor 10^{-3}-10^{-4}, after which all TOFs decline. The initial rise in the TOFs of CH_2O and CH_3OH results from improved adsorption of CH_3O and CH_3OO. Indeed, at high partial pressures of plasma species, the adsorption of CH_3O and CH_3OO is hindered by surface poisoning by stronger binding species, such as O* and coking species. By lowering the partial pressures of all plasma species, more free sites become available, i.e. the fraction of free surface sites increases from 10^{-10} to 10^{-5} when lowering the

partial pressures by a factor 10^{-6}. Moreover, the right panel of Figure 10 illustrates that the fractional coverages of coking precursors strongly decline as the partial pressures are lowered. The enhanced availability of free sites initially improves the adsorption of CH_3O and CH_3OO, even though their partial pressures are lower. As these species are precursors to CH_2O and CH_3OH, the TOFs of these products are higher. Upon further lowering the partial pressures of the plasma species, the TOFs eventually decrease due to the lower availability of reactive plasma species in the gas phase.

Our results thus show that lowering the radical densities in the plasma, up to a certain limit, is beneficial for oxygenate production, as this limits surface poisoning by strongly binding plasma species. This might be achieved by using a lower plasma power or placing a catalyst in the plasma afterglow. However, this might also change the radical distribution (in the plasma or afterglow). On the other hand, modelling of POX of CH_4 in a DBD shows that the densities of CH_3O and CH_3OO vary little between the pulses.[37] Therefore, these species are expected to remain among the most important radicals even in the afterglow.

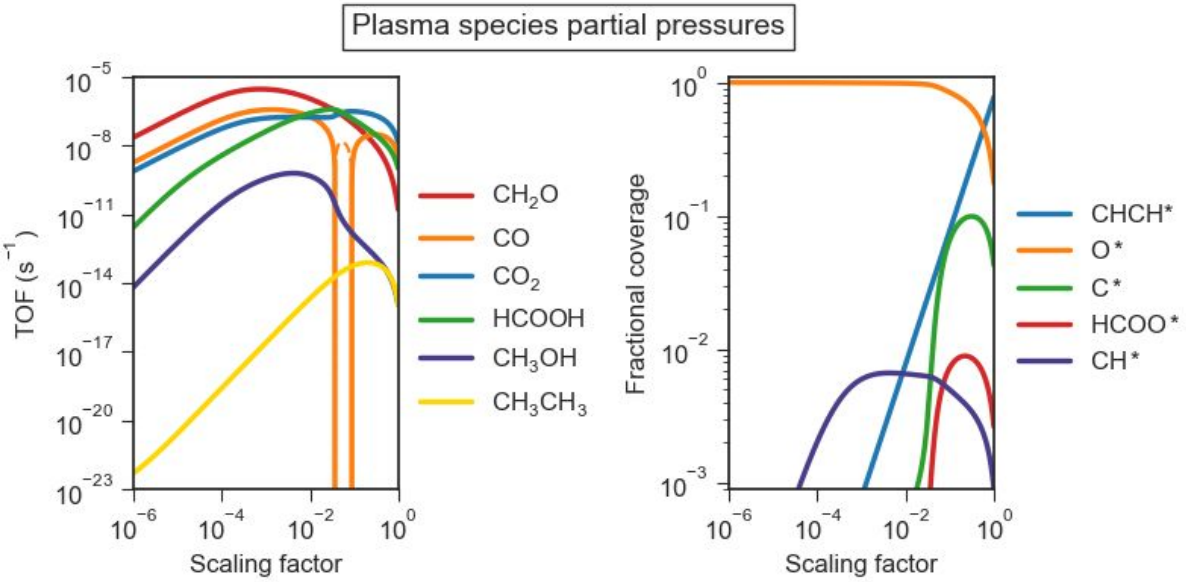

Figure 10. Influence of the partial pressures of all plasma-produced radicals and stable intermediates on TOFs (left) and surface coverages (right). Dotted lines in the left graph indicate consumption, whereas full lines indicate production. Calculated for a temperature of 500 K and a total pressure of 1 bar. The default values of the species partial pressures used in the simulations are shown in Table 1, but the partial pressures of all species, except for CH_4 and O_2, are simultaneously varied.

Figure 11 summarizes how the different plasma species discussed in this section affect the formation of CO_x and the oxygenates. Strongly dehydrogenated carbonaceous species, e.g. CHCH, CH and C, cause cokes formation on the catalyst surface and favour the production of CO over that of CO_2. O radicals, on the other hand, reduce coking but result in overoxidation to CO_2. The less strongly dehydrogenated carbonaceous species, i.e. CH_3 and CH_2, mainly

favour HCOOH, but also to a lesser extent cokes formation. H enhances the formation of HCOOH and CH_3OH by improving the hydrogenation of their respective precursor species, HCOO* and CH_3O*, and it also enhances the formation of CH_2O, by the higher adsorption of CH_3O, which can form both CH_3OH and CH_2O. The CH_3O and CH_3OO radicals are the precursors to both CH_3OH and CH_2O and thus also favour the formation of these products.

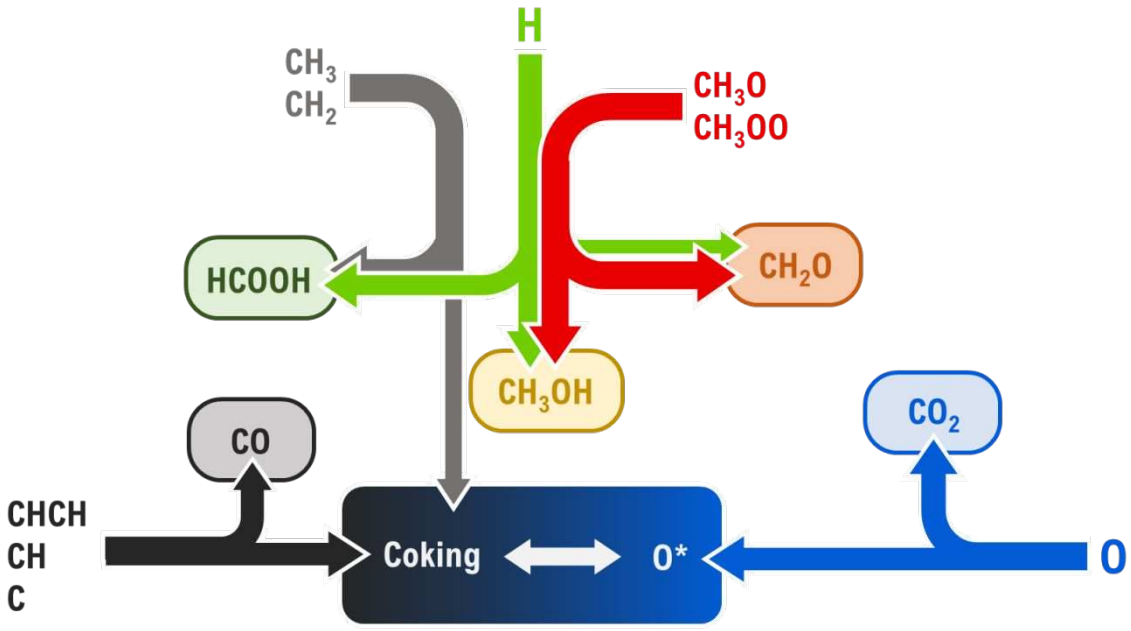

Figure 11. Overview of the influence of various plasma species on the formation of oxygenates and CO_x in the plasma-catalytic POX of CH_4 on Pt(111).

It should be noted that the present model focuses on the surface reactions, and the plasma chemistry is only taken as input. In future work, we plan to combine both the plasma chemistry and catalyst surface chemistry into one model, so that the effect of the surface reactions on the gas phase composition is self-consistently accounted for.

3.3.3. Eley-Rideal reactions involving radicals

Due to their highly reactive nature, radicals generally form strong bonds when adsorbing onto a catalysts surface. Together with the abundancy of radicals in the plasma, this can induce strong poisoning of the catalyst surface, as illustrated above. However, the high reactivity of plasma-generated radicals might also enable them to react with the surface species via Eley-Rideal (ER) reactions with low to zero enthalpy barriers. Therefore, we briefly illustrate the potential effect of these ER reactions by including the following three reactions in the chemistry set: $CH_3(g) + O^* \rightarrow CH_3O^*$, $H(g) + O^* \rightarrow OH^*$ and $O(g) + C^* \rightarrow CO^*$. We choose these reactions as CH_3, H and O are the main products of electron impact dissociation of CH_4 and O_2, respectively, and because O* and C* are abundant and simple surface species. To the best of

our knowledge, no activation barriers have been reported for these ER reactions. We therefore simultaneously vary the enthalpy barriers of these reactions between 0.0 and 0.75 eV. Higher enthalpy barriers show no further effect on the TOFs. For comparison, the ER reactions that involve CH_4 ($CH_4(g) + OH^* \rightarrow CH_3^* + H_2O^*$ and $CH_4(g) + O^* \rightarrow CH_3^* + OH^*$) have enthalpy barriers of 0.50 eV[71] and 1.28 eV[71], respectively. We would also like to emphasise that all ER reactions, including those with radicals, have an entropy barrier that corresponds to the loss of all translational entropy of the corresponding radical or gas molecule, as explained in the model description.

In Figure 12, we illustrate the influence of these ER reactions on the TOFs and surface coverages for the indicated range of enthalpy barriers. All the TOFs in Figure 12 rise upon lowering the enthalpy barriers and thus enhancing the importance of the ER reactions. For low barriers, CO becomes the main product due to the reactions of O radicals with surface C*. The TOFs of CH_2O and CH_3OH also rise strongly upon lowering the barriers, as a result of the enhanced formation of their precursor species, CH_3O^*, through reaction between $CH_3(g)$ and O*. Note that the net rate of CH_3O and CH_3OO adsorption/desorption is set to zero if desorption of these species occurs, thus assuming that an equilibrium is reached due to accumulation of these radicals near the surface. For the lower barriers (< 0.09 eV), CH_2O becomes the second most important product, after CO. The decomposition of CH_3O^* to CH_2O^* also forms H*, which enhances the formation of HCOOH and CH_3OH. Additionally, a drop in C* coverage and a rise in CH* coverage can be observed as a result of the improved H* formation.

In summary, our results show that ER reactions involving radicals have a potentially strong contribution to the TOFs in plasma catalysis. Additionally, these ER reactions might be responsible for a significant part of the oxygenate formation in plasma-catalytic POX of CH_4. We note that other ER reactions might also be important; however, the lack of reported activation energies currently limits the construction of an extended chemistry set with these reactions. The three ER reactions that we considered, are aimed at illustrating the potential impact of these reactions.

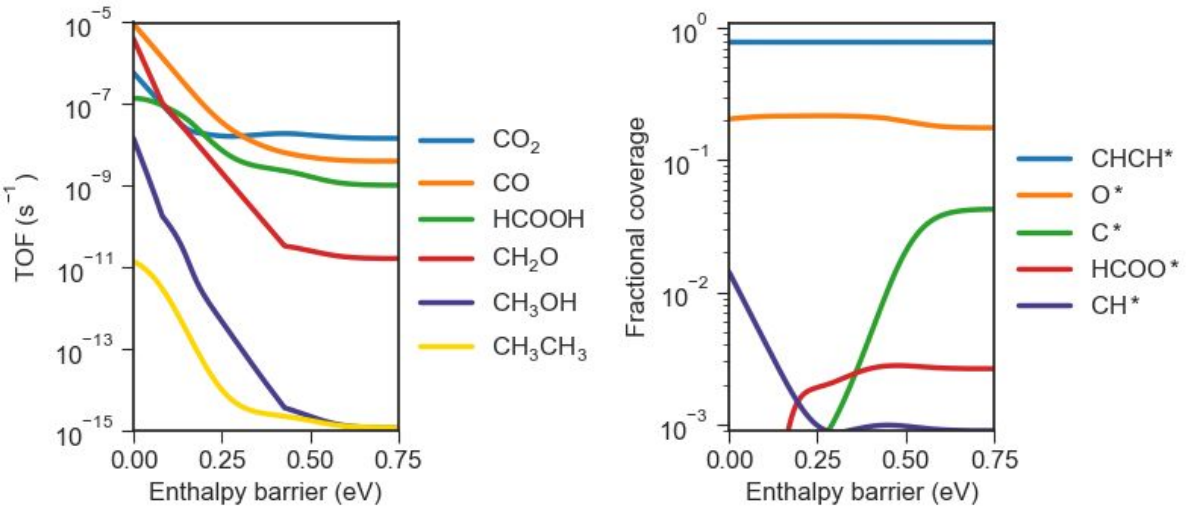

Figure 12. Influence of the enthalpy barriers of Eley-Rideal reactions involving radicals on the TOFs (left) and surface coverages (right). The following Eley-Rideal reactions are included: $CH_3(g) + O^* \rightarrow CH_3O^*$, $H(g) + O^* \rightarrow OH^*$ and $O(g) + C^* \rightarrow CO^*$, and their enthalpy barriers are simultaneously varied in the simulation. Calculated for a temperature of 500 K and a total pressure of 1 bar. The values of the species partial pressures used in the simulations are shown in Table 1.

3.4. Additional remarks and suggestions

3.4.1. Possible effect of C-C coupling reactions

As shown in Figures 5, 6 and 7, carbon-containing radicals can be present on the surface in high coverages. While high coverages of carbonaceous species like C*, CH* and CHCH* indicate that coking is likely to occur, our model does not explicitly capture the mechanism for coking. Additionally, C-C coupling to higher hydrocarbons might also become important under these conditions. While our model does contain some C-C coupling reactions to form C2 hydrocarbons, C-C coupling to higher hydrocarbons is not included, mainly due to lack of availability of the required thermodynamic input data in literature. Therefore, we should remain careful with the interpretation of our results under conditions where carbonaceous species appear to poison the surface. If C-C coupling to higher hydrocarbons would be favoured over cokes formation, then formation and desorption of these higher hydrocarbons might result in an improved availability of free sites and higher TOFs. However, this also depends on the barrier for desorption of the formed product. Nevertheless, we would like to emphasise that the main focus of this study is on the formation of oxygenates under partial oxidation conditions, where oxidation reactions are the dominant mechanism.

3.4.2. Other catalyst materials

Our model is applied to Pt(111)), but we provide here some information on how (or whether) our results might be translated to other catalyst materials, based on insights obtained from our work and literature. Microkinetic modelling of the thermal-catalytic POX of CH_4 by Yoo *et*

al.[40] shows that for Pt-group metals the selectivity of CH_2O increases when going towards metals that bind O* more strongly. This was attributed to the higher O* coverages, which promote the coupling between CH_3* and O* to form CH_3O*, and the subsequent O*-assisted dehydrogenation of CH_3O* to CH_2O*.[40] While for plasma conditions where CH_3O* can be formed in the plasma itself, we can expect that metals with a higher O*-binding strength, such as Pd and Rh, improve the adsorption of CH_3O* and CH_3OO* to the surface, thus also enhancing CH_2O, and possibly CH_3OH formation. Yoo *et al*.[40] also found that coinage metals, such as Cu, Ag and Au, are most suitable catalysts for CH_2O and CH_3OH synthesis. The authors determined that the selectivity of CH_2O vs. CH_3OH on these catalysts was determined by competition between two reaction paths: $CH_3* + O* \rightarrow CH_3O*$ (following dehydrogenation to CH_2O*) and $CH_3* + OH* \rightarrow CH_3OH*$.[40] For plasma catalysis we might thus also expect a change in the mechanism of CH_3OH* formation, where CH_3 and OH radicals become the main precursors for CH_3OH on the most noble metals. In this case it might be possible to steer the selectivity of CH_2O vs. CH_3OH by changing the densities of O vs OH radicals in the plasma.

Using DFT and microkinetic modelling, Studt *et al.*[72] illustrated the effect of alloying Cu with ZnO for thermal-catalytic hydrogenation of CO and CO_2. Zn results in stronger O-binding and weaker C-binding. The former enhances CO_2 hydrogenation by stabilizing the O*-bound intermediates, such as HCOO*, while the latter results in more difficult adsorption and hydrogenation of CO.[72] Applied to our results, this catalyst might also be beneficial for plasma catalysis, because stronger O-binding might result in less desorption and formation of CO_2 and more facile hydrogenation of HCOO* to HCOOH or other oxygenates, and weaker C-binding is expected to result in less adsorption and oxidation of plasma-produced CO.

Certain metal oxides, such as MoO_3 and V_2O_5, may also be suitable catalysts for the production of CH_2O and CH_3OH by plasma-catalytic POX. CH_3 radicals can react with reducible metal oxides to form methoxide anions (CH_3O^-) on the surface, as was shown by Tong *et al*.[73] (Note the similarities with the Eley-Rideal reaction $CH_3 + O* \rightarrow CH_3O*$, discussed in section 3.3.3.) The reactivity of the metal oxide in this reaction depends on its reducibility, with more reducible metal oxides being more reactive. On CeO_2, the formed CH_3O^- anion reacts into a formate anion ($HCOO^-$), which produces CO and CO_2.[73] However, on MoO_3 and V_2O_5 the CH_3O^- anion can react to produce CH_2O or, in case H_2O is present, CH_3OH.[74,75] Additionally, MoO_3 and V_2O_5 are known catalysts for the selective O-insertion into CH_3 in thermal-catalytic POX of CH_4 to CH_2O and CH_3OH. In this reaction NO is typically added as a radical initiator.[76] As high

densities of radicals, such as CH_3, can easily be achieved in plasma, the combination of a MoO_3 or V_2O_5 catalyst with plasma also seems promising for plasma-catalytic POX of CH_4.

4. Conclusion

We used microkinetic modelling to investigate the influence of various plasma species on the catalyst surface chemistry for plasma-catalytic POX of CH_4 on a Pt(111) surface. We evaluated the effect of vibrationally excited CH_4 and O_2, as well as, radicals and stable intermediates, and compared the results to those of thermal catalysis at the same reaction conditions.

Plasma-induced vibrational excitation of CH_4 and O_2 increases the TOF of CH_4 dissociation. Furthermore, it also shows potential for enhancing the selectivities of CH_3OH, HCOOH and C_2 hydrocarbons, but has little effect on the selectivities of CH_2O, CO and CO_2. Nevertheless, the selectivities of CH_3OH, CH_2O and C_2 hydrocarbons remain too low for their production to be feasible on Pt(111) at conditions when only vibrational excitation is considered as a plasma-effect. However, we find that for plasma-catalytic POX of CH_4 the surface chemistry is mainly governed by radicals, rather than vibrationally excited molecules.

The presence of plasma-produced radicals and stable intermediates greatly increases the TOFs of CO_x and the oxygenates, compared to thermal catalysis. Interestingly, it also enhances the selectivities of the oxygenates and we find that the production of HCOOH becomes non-negligible. Further, we examine the role of various radicals in the surface processes:

- O radicals counteract coking, but also promote deep oxidation to CO_2 and their partial pressures should be tuned against that of carbonaceous radicals.
- Strongly dehydrogenated carbonaceous species (CHCH, CH, C) are found to strongly induce coking, and their formation should be avoided.
- The more hydrogenated carbonaceous radicals (CH_3, CH_2) show in general a beneficial effect, as they bind less strongly to the catalyst and lead to H* formation on the surface, yet also cause coking at high partial pressures.
- H radicals appear beneficial by promoting the hydrogenation of CH_3O* and HCOO* to CH_3OH and HCOOH, respectively. Moreover, high partial pressures of H radicals can potentially form more free surface sites by removing excess O* via H_2O formation.
- CH_3O and CH_3OO radicals are important precursors to both CH_3OH and CH_2O. Increasing their partial pressures thus also strongly enhances CH_3OH and CH_2O formation.

- Lowering the radical partial pressures in general decreases surface poisoning and allows for more facile adsorption of weak-binding radicals (e.g. CH_3O and CH_3OO), which is beneficial for oxygenate formation.

Based on the effects of these radicals we make the following suggestions on which reaction conditions should be used to favour the formation of certain products:

- The formation of undesired CO_2 is favoured at low CH_4/O_2 ratios, for which high partial pressures of O radicals are expected. While such conditions should generally be avoided to limit deep oxidation, these can also be beneficial to some extent by avoiding coke formation.
- The formation of CO is favoured at high CH_4/O_2 ratios and might to some extent also benefit from a higher plasma power, that yields stronger CH_4 dissociation, although caution must be taken to avoid excessive carbon deposition on the surface.
- HCOOH formation benefits from the presence of CH_3 and CH_2 radicals, which are expected to be abundant in plasmas with a high CH_4/O_2 ratio and lower plasma power, avoiding complete CH_4 dissociation. An additional H source, such as H_2, might also be beneficial by improving HCOO* hydrogenation.
- The formation of CH_3OH might also benefit from a lower plasma power, resulting in lower radical densities (especially of strong binding carbonaceous species) and more free sites, which enhances CH_3O and CH_3OO adsorption. Additionally, CH_3O hydrogenation is expected to improve from using H_2 as additional H source in the plasma or a more noble catalyst.
- The formation of CH_2O is also expected to benefit from lower plasma power, for the same reason as CH_3OH. Moreover, an additional H source can also partially enhance CH_2O formation, as it can help to clear the surface from excessive O*.

Finally, we briefly illustrate the potential impact of Eley-Rideal reactions that involve radicals. We find that these reactions allow to reach high TOFs, even at the high surface coverages that are relevant for plasma catalysis. Additionally, these reactions might lead to significant oxygenate production in the plasma-catalytic POX of CH_4 due to reactions such as $CH_3(g) + O^* \rightarrow CH_3O^*$, that result in more direct routes towards oxygenates.

Supporting Information

List of reactions included in the model; thermal-catalytic pathway at 1000 K and comparison with literature; Effect of CO concentration on CO_2 selectivity; Influence of vibrational excitation on the surface coverages and on the selectivities of CH_2CH_2 and CHCH; Influence of vibrational excitation on TOF's in the presence of radicals; Effect of OH & OOH, COOH and HCOO radicals on TOFs and coverages

Acknowledgments

We would like to thank Tom Butterworth for the interesting discussions regarding the calculation of the vibrational populations of methane and for taking the time to share his thoughts and experiences on the matter. This research is supported by the FWO-SBO project PLASMACATDesign (grant number S001619N). We also acknowledge financial support from the TOP-BOF project of the University of Antwerp and from the European Research Council (ERC) under the European Union's Horizon 2020 research and innovation program (grant agreement No 810182 – SCOPE ERC Synergy project). The calculations were carried out using the Turing HPC infrastructure at the CalcUA core facility of the Universiteit Antwerpen, a division of the Flemish Supercomputer Center VSC, funded by the Hercules Foundation, the Flemish Government (Department EWI), and the University of Antwerp.

5. References

(1) Olivos-Suarez, A. I.; Szécsényi, À.; Hensen, E. J. M.; Ruiz-Martinez, J.; Pidko, E. A.; Gascon, J. Strategies for the Direct Catalytic Valorization of Methane Using Heterogeneous Catalysis: Challenges and Opportunities. *ACS Catal.* **2016**, *6*, 2965–2981.

(2) Schwach, P.; Pan, X.; Bao, X. Direct Conversion of Methane to Value-Added Chemicals over Heterogeneous Catalysts: Challenges and Prospects. *Chem. Rev.* **2017**, *117*, 8497–8520.

(3) Zakaria, Z.; Kamarudin, S. K. Direct Conversion Technologies of Methane to Methanol: An Overview. *Renewable Sustainable Energy Rev.* **2016**, *65*, 250–261.

(4) Nozaki, T.; Ağıral, A.; Yuzawa, S.; Gardeniers, J. G. E. H.; Okazaki, K. A Single Step Methane Conversion into Synthetic Fuels Using Microplasma Reactor. *Chem. Eng. J.* **2011**, *166*, 288–293.

(5) Ravi, M.; Ranocchiari, M.; van Bokhoven, J. A. The Direct Catalytic Oxidation of Methane to Methanol-A Critical Assessment. *Angew. Chem., Int. Ed.* **2017**, *56*, 16464–16483.

(6) Dinh, K. T.; Sullivan, M. M.; Serna, P.; Meyer, R. J.; Dincă, M.; Román-Leshkov, Y. Viewpoint on the Partial Oxidation of Methane to Methanol Using Cu- and Fe-Exchanged Zeolites. *ACS Catal.* **2018**, *8*, 8306–8313.

(7) Karakaya, C.; Kee, R. J. Progress in the Direct Catalytic Conversion of Methane to Fuels and Chemicals. *Prog. Energy Combust. Sci.* **2016**, *55*, 60–97.

(8) Enger, B. C.; Lødeng, R.; Holmen, A. A Review of Catalytic Partial Oxidation of Methane to Synthesis Gas with Emphasis on Reaction Mechanisms over Transition Metal Catalysts. *Appl. Catal. A* **2008**, *346*, 1–27.

(9) Goujard, V.; Nozaki, T.; Yuzawa, S.; Ağiral, A.; Okazaki, K. Plasma-Assisted Partial Oxidation of Methane at Low Temperatures: Numerical Analysis of Gas-Phase Chemical Mechanism. *J. Phys. D: Appl. Phys.* **2011**, *44*, 274011.

(10) Snoeckx, R.; Bogaerts, A. Plasma Technology - a Novel Solution for CO_2 Conversion? *Chem. Soc. Rev.* **2017**, *46*, 5805–5863.

(11) Bogaerts, A.; Tu, X.; Whitehead, J. C.; Centi, G.; Lefferts, L.; Guaitella, O.; Azzolina-Jury, F.; Kim, H.-H.; Murphy, A. B.; Schneider, W. F.; et al. The 2020 Plasma Catalysis Roadmap. *J. Phys. D: Appl. Phys.* **2020**, *53*, 443001.

(12) Neyts, E. C.; Ostrikov, K. K.; Sunkara, M. K.; Bogaerts, A. Plasma Catalysis: Synergistic Effects at the Nanoscale. *Chem. Rev.* **2015**, *115*, 13408–13446.

(13) *Plasma Catalysis*; Tu, X., Whitehead, J. C., Nozaki, T., Eds.; Springer International Publishing: Cham, 2019.

(14) Ağıral, A.; Nozaki, T.; Nakase, M.; Yuzawa, S.; Okazaki, K.; Gardeniers, J. G. E. H. Gas-to-Liquids Process Using Multi-Phase Flow, Non-Thermal Plasma Microreactor. *Chem. Eng. J.* **2011**, *167*, 560–566.

(15) Hoeben, W. F. L. M.; Boekhoven, W.; Beckers, F. J. C. M.; Van Heesch, E. J. M.; Pemen, A. J. M. Partial Oxidation of Methane by Pulsed Corona Discharges. *J. Phys. D: Appl. Phys.* **2014**, *47*, 355202.

(16) Huang, J.; Badani, M. V.; Suib, S. L.; Harrison, J. B.; Kablauoi, M. Partial Oxidation of Methane to Methanol through Microwave Plasmas. Reactor Design to Control Free-Radical Reactions. *J. Phys. Chem.* **1994**, *98*, 206–210.

(17) Kalra, C. S.; Gutsol, A. F.; Fridman, A. A. Gliding Arc Discharges as a Source of Intermediate Plasma for Methane Partial Oxidation. *IEEE Trans. Plasma Sci.* **2005**, *33*, 32–41.

(18) Nair, S. A.; Nozaki, T.; Okazaki, K. Methane Oxidative Conversion Pathways in a Dielectric Barrier Discharge Reactor—Investigation of Gas Phase Mechanism. *Chem. Eng. J.* **2007**, *132*, 85–95.

(19) Nozaki, T.; Hattori, A.; Okazaki, K. Partial Oxidation of Methane Using a Microscale Non-Equilibrium Plasma Reactor. *Catal. Today* **2004**, *98*, 607–616.

(20) Wang, Y.-F.; Tsai, C.-H.; Shih, M.; Hsieh, L.-T.; Chang, W. Direct Conversion of Methane into Methanol and Formaldehyde in an RF Plasma Environment II: Effects of Experimental Parameters. *Aerosol Air Qual. Res.* **2005**, *5*, 211–224.

(21) Kogelschatz, U. Dielectric-Barrier Discharges: Their History, Discharge Physics, and Industrial Applications. *Plasma Chem. Plasma Process.* **2003**, *23*, 1–46.

(22) Chawdhury, P.; Ray, D.; Vinodkumar, T.; Subrahmanyam, C. Catalytic DBD Plasma Approach for Methane Partial Oxidation to Methanol under Ambient Conditions. *Catal. Today* **2019**, *337*, 117–125.

(23) Chen, L.; Zhang, X.; Huang, L.; Lei, L. Application of In-Plasma Catalysis and Post-Plasma Catalysis for Methane Partial Oxidation to Methanol over a Fe_2O_3-CuO/γ-Al_2O_3 Catalyst. *J. Nat. Gas Chem.* **2010**, *19*, 628–637.

(24) Huang, L.; Zhang, X.; Chen, L.; Lei, L. Direct Oxidation of Methane to Methanol Over Cu-Based Catalyst in an AC Dielectric Barrier Discharge. *Plasma Chem. Plasma Process.* **2011**, *31*, 67–77.

(25) Chen, L.; Zhang, X.-W.; Huang, L.; Lei, L.-C. Partial Oxidation of Methane with Air for Methanol Production in a Post-Plasma Catalytic System. *Chem. Eng. Process.* **2009**, *48*, 1333–1340.

(26) Lee, H.; Kim, D. H. Direct Methanol Synthesis from Methane in a Plasma-Catalyst Hybrid System at Low Temperature Using Metal Oxide-Coated Glass Beads. *Sci. Rep.*

2018, *8*, 9956.

(27) Indarto, A. Methanol Synthesis from Methane and Oxygen with [Ga Cr]/Cu–Zn–Al Catalyst in a Dielectric Barrier Discharge. *Ionics* **2014**, *20*, 445–449.

(28) Indarto, A.; Yang, D. R.; Palgunadi, J.; Choi, J.-W.; Lee, H.; Song, H. K. Partial Oxidation of Methane with Cu–Zn–Al Catalyst in a Dielectric Barrier Discharge. *Chem. Eng. Process.* **2008**, *47*, 780–786.

(29) Heintze, M.; Pietruszka, B. Plasma Catalytic Conversion of Methane into Syngas: The Combined Effect of Discharge Activation and Catalysis. *Catal. Today* **2004**, *89*, 21–25.

(30) Indarto, A.; Lee, H.; Choi, J.-W.; Song, H. K. Partial Oxidation of Methane with Yttria-Stabilized Zirconia Catalyst in a Dielectric Barrier Discharge. *Energy Sources, Part A* **2008**, *30*, 1628–1636.

(31) Pietruszka, B.; Anklam, K.; Heintze, M. Plasma-Assisted Partial Oxidation of Methane to Synthesis Gas in a Dielectric Barrier Discharge. *Appl. Catal. A* **2004**, *261*, 19–24.

(32) Jurković, D. L.; Puliyalil, H.; Pohar, A.; Likozar, B. Plasma-Activated Methane Partial Oxidation Reaction to Oxygenate Platform Chemicals over Fe, Mo, Pd and Zeolite Catalysts. *Int. J. Energy Res.* **2019**, *43*, 8085–8099.

(33) Knoll, A. J.; Zhang, S.; Lai, M.; Luan, P.; Oehrlein, G. S. Infrared Studies of Gas Phase and Surface Processes of the Enhancement of Catalytic Methane Decomposition by Low Temperature Plasma. *J. Phys. D: Appl. Phys.* **2019**, *52*, 225201.

(34) Zhang, S.; Li, Y.; Knoll, A.; Oehrlein, G. S. Mechanistic Aspects of Plasma-Enhanced Catalytic Methane Decomposition by Time-Resolved Operando Diffuse Reflectance Infrared Fourier Transform Spectroscopy. *J. Phys. D: Appl. Phys.* **2020**, *53*, 215201.

(35) Gibson, E. K.; Stere, C. E.; Curran-McAteer, B.; Jones, W.; Cibin, G.; Gianolio, D.; Goguet, A.; Wells, P. P.; Catlow, C. R. A.; Collier, P.; et al. Probing the Role of a Non-Thermal Plasma (NTP) in the Hybrid NTP Catalytic Oxidation of Methane. *Angew. Chem., Int. Ed.* **2017**, *56*, 9351–9355.

(36) Stere, C.; Chansai, S.; Gholami, R.; Wangkawong, K.; Singhania, A.; Goguet, A.; Inceesungvorn, B.; Hardacre, C. A Design of a Fixed Bed Plasma DRIFTS Cell for Studying the NTP-Assisted Heterogeneously Catalysed Reactions. *Catal. Sci. Technol.* **2020**, *10*, 1458–1466.

(37) De Bie, C.; van Dijk, J.; Bogaerts, A. The Dominant Pathways for the Conversion of Methane into Oxygenates and Syngas in an Atmospheric Pressure Dielectric Barrier Discharge. *J. Phys. Chem. C* **2015**, *119*, 22331–22350.

(38) Qian, M.; Zhong, W.; Kang, J.; Liu, S.; Ren, C.; Zhang, J.; Wang, D. Global Modeling on Partial Oxidation of Methane to Oxygenates and Syngas in Non-Equilibrium Plasma. *Jpn. J. Appl. Phys.* **2020**, *59*, 066003.

(39) Olivera, P. P.; Patrito, E. M.; Sellers, H. Direct Synthesis of Methanol over Metallic Catalysts. *Surf. Sci.* **1995**, *327*, 330–357.

(40) Yoo, J. S.; Schumann, J.; Studt, F.; Abild-Pedersen, F.; Nørskov, J. K. Theoretical Investigation of Methane Oxidation on Pd(111) and Other Metallic Surfaces. *J. Phys. Chem. C* **2018**, *122*, 16023–16032.

(41) Xing, B.; Pang, X.-Y.; Wang, G.-C. C–H Bond Activation of Methane on Clean and Oxygen Pre-Covered Metals: A Systematic Theoretical Study. *J. Catal.* **2011**, *282*, 74–82.

(42) Baek, B.; Aboiralor, A.; Wang, S.; Kharidehal, P.; Grabow, L. C.; Massa, J. D. Strategy to Improve Catalytic Trend Predictions for Methane Oxidation and Reforming. *AIChE J.* **2017**, *63*, 66–77.

(43) Mehta, P.; Barboun, P.; Go, D. B.; Hicks, J. C.; Schneider, W. F. Catalysis Enabled by Plasma Activation of Strong Chemical Bonds: A Review. *ACS Energy Lett.* **2019**, *4*, 1115–1133.

(44) Mehta, P.; Barboun, P.; Herrera, F. A.; Kim, J.; Rumbach, P.; Go, D. B.; Hicks, J. C.; Schneider, W. F. Overcoming Ammonia Synthesis Scaling Relations with Plasma-Enabled Catalysis. *Nat. Catal.* **2018**, *1*, 269–275.

(45) Engelmann, Y.; Mehta, P.; Neyts, E. C.; Schneider, W. F.; Bogaerts, A. Predicted Influence of Plasma Activation on Nonoxidative Coupling of Methane on Transition Metal Catalysts. *ACS Sustain. Chem. Eng.* **2020**, *8*, 6043–6054.

(46) Michiels, R.; Engelmann, Y.; Bogaerts, A. Plasma Catalysis for CO_2 Hydrogenation: Unlocking New Pathways toward CH_3OH. *J. Phys. Chem. C* **2020**, *124*, 25859–25872.

(47) York, A. P. E.; Xiao, T.; Green, M. L. H. Brief Overview of the Partial Oxidation of Methane to Synthesis Gas. *Top. Catal.* **2003**, *22*, 345–358.

(48) Liu, C.; Li, M.; Wang, J.; Zhou, X.; Guo, Q.; Yan, J.; Li, Y. Plasma Methods for Preparing Green Catalysts: Current Status and Perspective. *Chin. J. Catal.* **2016**, *37*, 340–348.

(49) Kraus, P.; Lindstedt, R. P. Microkinetic Mechanisms for Partial Oxidation of Methane over Platinum and Rhodium. *J. Phys. Chem. C* **2017**, *121*, 9442–9453.

(50) Mhadeshwar, A. B.; Vlachos, D. G. A Catalytic Reaction Mechanism for Methane Partial Oxidation at Short Contact Times, Reforming, and Combustion, and for Oxygenate Decomposition and Oxidation on Platinum. *Ind. Eng. Chem. Res.* **2007**, *46*, 5310–5324.

(51) Korup, O.; Goldsmith, C. F.; Weinberg, G.; Geske, M.; Kandemir, T.; Schlögl, R.; Horn, R. Catalytic Partial Oxidation of Methane on Platinum Investigated by Spatial Reactor Profiles, Spatially Resolved Spectroscopy, and Microkinetic Modeling. *J. Catal.* **2013**, *297*, 1–16.

(52) Aghalayam, P.; Park, Y. K.; Fernandes, N.; Papavassiliou, V.; Mhadeshwar, A. B.; Vlachos, D. G. A C1 Mechanism for Methane Oxidation on Platinum. *J. Catal.* **2003**, *213*, 23–38.

(53) Chen, Y.; Vlachos, D. G. Density Functional Theory Study of Methane Oxidation and Reforming on Pt(111) and Pt(211). *Ind. Eng. Chem. Res.* **2012**, *51*, 12244−12252.

(54) Wang, R.; Chen, J.; Zhao, W.; Wen, J.; Li, H.; Li, L.; Ran, J. Mechanism of the Catalytic Oxidation of Methane on Pt(1 1 1) Surfaces in Moist Environment: A Density Functional Theory Study. *Appl. Surf. Sci.* **2019**, *471*, 566–586.

(55) Nørskov, J. K.; Studt, F.; Abild-Pedersen, F.; Bligaard, T. *Fundamental Concepts in Heterogeneous Catalysis*; John Wiley & Sons, Inc.: Hoboken, New Jersey, 2014.

(56) Campbell, C. T.; Sprowl, L. H.; Árnadóttir, L. Equilibrium Constants and Rate Constants for Adsorbates: Two-Dimensional (2D) Ideal Gas, 2D Ideal Lattice Gas, and Ideal Hindered Translator Models. *J. Phys. Chem. C* **2016**, *120*, 10283–10297.

(57) Bitsch-Larsen, A.; Horn, R.; Schmidt, L. D. Catalytic Partial Oxidation of Methane on Rhodium and Platinum: Spatial Profiles at Elevated Pressure. *Appl. Catal. A* **2008**, *348*, 165–172.

(58) Horn, R.; Williams, K.; Degenstein, N.; Bitsch-Larsen, A.; Dalle Nogare, D.; Tupy, S.; Schmidt, L. Methane Catalytic Partial Oxidation on Autothermal Rh and Pt Foam

Catalysts: Oxidation and Reforming Zones, Transport Effects, and Approach to Thermodynamic Equilibrium. *J. Catal.* **2007**, *249*, 380–393.

(59) Chin, Y.-H. C.; Buda, C.; Neurock, M.; Iglesia, E. Selectivity of Chemisorbed Oxygen in C–H Bond Activation and CO Oxidation and Kinetic Consequences for CH_4–O_2 Catalysis on Pt and Rh Clusters. *J. Catal.* **2011**, *283*, 10–24.

(60) Chin, Y.-H.; Buda, C.; Neurock, M.; Iglesia, E. Reactivity of Chemisorbed Oxygen Atoms and Their Catalytic Consequences during CH_4 –O_2 Catalysis on Supported Pt Clusters. *J. Am. Chem. Soc.* **2011**, *133*, 15958–15978.

(61) Maitre, P.-A.; Bieniek, M. S.; Kechagiopoulos, P. N. Plasma-Enhanced Catalysis for the Upgrading of Methane: A Review of Modelling and Simulation Methods. *React. Chem. Eng.* **2020**, *5*, 814–837.

(62) Chen, T. Y.; Rousso, A. C.; Wu, S.; Goldberg, B. M.; van der Meiden, H.; Ju, Y.; Kolemen, E. Time-Resolved Characterization of Plasma Properties in a CH_4/He Nanosecond-Pulsed Dielectric Barrier Discharge. *J. Phys. D: Appl. Phys.* **2019**, *52*, 18LT02.

(63) Butterworth, T.; van de Steeg, A.; van den Bekerom, D.; Minea, T.; Righart, T.; Ong, Q.; van Rooij, G. Plasma Induced Vibrational Excitation of CH_4 —a Window to Its Mode Selective Processing. *Plasma Sources Sci. Technol.* **2020**, *29*, 095007.

(64) Shen, X.; Liu, W.; Gao, X.; Lu, Z.; Wu, X.; Gao, X. Mechanisms of Oxidase and Superoxide Dismutation-like Activities of Gold, Silver, Platinum, and Palladium, and Their Alloys: A General Way to the Activation of Molecular Oxygen. *J. Am. Chem. Soc.* **2015**, *137*, 15882–15891.

(65) Du, Y.; Nayak, G.; Oinuma, G.; Peng, Z.; Bruggeman, P. J. Effect of Water Vapor on Plasma Morphology, OH and H_2O_2 Production in He and Ar Atmospheric Pressure Dielectric Barrier Discharges. *J. Phys. D: Appl. Phys.* **2017**, *50*, 145201.

(66) Snoeckx, R.; Ozkan, A.; Reniers, F.; Bogaerts, A. The Quest for Value-Added Products from Carbon Dioxide and Water in a Dielectric Barrier Discharge: A Chemical Kinetics Study. *ChemSusChem* **2017**, *10*, 409–424.

(67) Vasko, C. A.; Liu, D. X.; van Veldhuizen, E. M.; Iza, F.; Bruggeman, P. J. Hydrogen Peroxide Production in an Atmospheric Pressure RF Glow Discharge: Comparison of

Models and Experiments. *Plasma Chem. Plasma Process.* **2014**, *34*, 1081–1099.

(68) Nunnally, T.; Gutsol, K.; Rabinovich, A.; Fridman, A.; Gutsol, A.; Kemoun, A. Dissociation of CO_2 in a Low Current Gliding Arc Plasmatron. *J. Phys. D: Appl. Phys.* **2011**, *44*, 274009.

(69) Larkin, D. W.; Zhou, L.; Lobban, L. L.; Mallinson, R. G. Product Selectivity Control and Organic Oxygenate Pathways from Partial Oxidation of Methane in a Silent Electric Discharge Reactor. *Ind. Eng. Chem. Res.* **2001**, *40*, 5496–5506.

(70) Larkin, D. W.; Lobban, L. L.; Mallinson, R. G. The Direct Partial Oxidation of Methane to Organic Oxygenates Using a Dielectric Barrier Discharge Reactor as a Catalytic Reactor Analog. *Catal. Today* **2001**, *71*, 199–210.

(71) Chen, Y.; Vlachos, D. G. Hydrogenation of Ethylene and Dehydrogenation and Hydrogenolysis of Ethane on Pt(111) and Pt(211): A Density Functional Theory Study. *J. Phys. Chem. C* **2010**, *114*, 4973–4982.

(72) Studt, F.; Behrens, M.; Kunkes, E. L.; Thomas, N.; Zander, S.; Tarasov, A.; Schumann, J.; Frei, E.; Varley, J. B.; Abild-Pedersen, F.; et al. The Mechanism of CO and CO_2 Hydrogenation to Methanol over Cu-Based Catalysts. *ChemCatChem* **2015**, *7*, 1105–1111.

(73) Tong, Y.; Lunsford, J. H. Mechanistic and Kinetic Studies of the Reactions of Gas-Phase Methyl Radicals with Metal Oxides. *J. Am. Chem. Soc.* **1991**, *113*, 4741–4746.

(74) Pak, S.; Smith, C. E.; Rosynek, M. P.; Lunsford, J. H. Conversion of Methyl Radicals to Methanol and Formaldehyde over Vanadium Oxide Catalysts. *J. Catal.* **1997**, *165*, 73–79.

(75) Pak, S.; Rosynek, M. P.; Lunsford, J. H. Conversion of Methyl Radicals to Methanol and Formaldehyde over Molybdenum Oxide Catalysts. *J. Phys. Chem.* **1994**, *98*, 11786–11790.

(76) Alvarez-Galvan, M. C.; Mota, N.; Ojeda, M.; Rojas, S.; Navarro, R. M.; Fierro, J. L. G. Direct Methane Conversion Routes to Chemicals and Fuels. *Catal. Today* **2011**, *171*, 15–23.

TOC Graphic

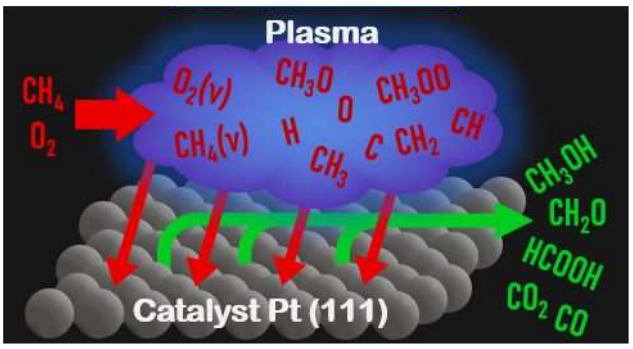
Plasma
CH_4
O_2
$O_2(v)$
$CH_4(v)$
CH_3O
CH_3OO
O
H
CH_3
C
CH_2
CH
CH_3OH
CH_2O
HCOOH
CO_2 CO
Catalyst Pt (111)